Article

Spectroscopic Investigation of Stellacyanin Mutants: Axial Ligand Interactions at the Blue Copper Site

Serena DeBeer George, Lipika Basumallick, Robert K. Szilagyi, David W. Randall, Michael G. Hill, Aram M. Nersissian, Joan S. Valentine, Britt Hedman, Keith O. Hodgson, and Edward I. Solomon

J. Am. Chem. Soc., **2003**, 125 (37), 11314-11328• DOI: 10.1021/ja035802j • Publication Date (Web): 19 August 2003

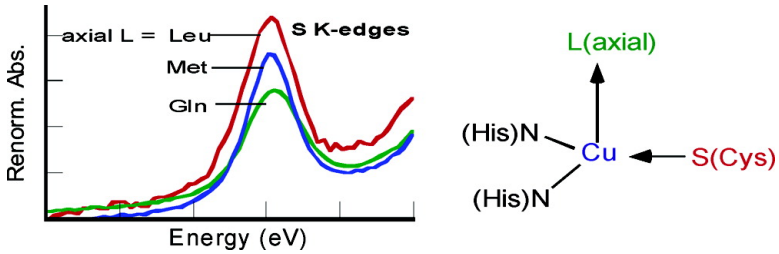

More About This Article

Additional resources and features associated with this article are available within the HTML version:

- Supporting Information
- Links to the 8 articles that cite this article, as of the time of this article download
- Access to high resolution figures
- Links to articles and content related to this article
- Copyright permission to reproduce figures and/or text from this article

View the Full Text HTML

J|A|C|S
ARTICLES
Published on Web 08/19/2003

Spectroscopic Investigation of Stellacyanin Mutants: Axial Ligand Interactions at the Blue Copper Site

Serena DeBeer George,[†,‡] Lipika Basumallick,[†] Robert K. Szilagyi,[†] David W. Randall,[†] Michael G. Hill,[§] Aram M. Nersissian,[||] Joan S. Valentine,[||] Britt Hedman,[*,†,‡] Keith O. Hodgson,[*,†,‡] and Edward I. Solomon[*,†]

Contribution from the Department of Chemistry, Stanford University, Stanford, California 94305, Stanford Synchrotron Radiation Laboratory, SLAC, Stanford University, Stanford, California 94309, Department of Chemistry, Occidental College, Los Angeles, California 90041, and Department of Chemistry and Biochemistry, University of California, Los Angeles, California 91125

Received April 25, 2003; E-mail: edward.solomon@stanford.edu

Abstract: Detailed electronic and geometric structural descriptions of the blue copper sites in wild-type (WT) stellacyanin and its Q99M and Q99L axial mutants have been obtained using a combination of XAS, resonance Raman, MCD, EPR, and DFT calculations. The results show that the origin of the short Cu−S(Cys) bond in blue copper proteins is the weakened axial interaction, which leads to a shorter (based on EXAFS results) and more covalent (based on S K-edge XAS) Cu−S bond. XAS pre-edge energies show that the effective nuclear charge on the copper increases going from O(Gln) to S(Met) to no axial (Leu) ligand, indicating that the weakened axial ligand is not fully compensated for by the increased donation from the thiolate. This is further supported by EPR results. MCD data show that the decreased axial interaction leads to an increase in the equatorial ligand field, indicating that the site acquires a more trigonally distorted tetrahedral structure. These geometric and electronic structural changes, which result from weakening the bonding interaction of the axial ligand, allow the site to maintain efficient electron transfer (high H_{DA} and low reorganization energy), while modulating the redox potential of the site to the biologically relevant range. These spectroscopic studies are complemented by DFT calculations to obtain insight into the factors that allow stellacyanin to maintain a trigonally distorted tetrahedral structure with a relatively strong axial Cu(II)−oxygen bond.

I. Introduction

Blue copper proteins are characterized by high-redox potentials, rapid electron-transfer rates, and unique spectral features as compared to "normal" tetragonal copper complexes.[1−8] The unique spectral features include an intense absorption band at ~600 nm and a small $A_{||}$ value in the EPR spectrum,[8,9] which derive from the highly covalent Cu−S(Cys) π bond.[10] A direct experimental measure of the Cu−S(Cys) covalency has been obtained through S K-edge measurements on plastocyanin, which indicate that there is 38% S(Cys) π character in the Cu $d_{x^2-y^2}$ orbital.[11] This covalency can provide strong electronic coupling into protein pathways to facilitate rapid long-range electron transfer;[12] hence an understanding of the factors which can modulate the covalency of the Cu−S(thiolate) bond is of significant interest.

It has been proposed that the highly covalent Cu−S(Cys) bond derives from the geometric structure of blue copper sites.[10] The classic blue copper sites, such as azurin and plastocyanin, have a single Cu ion in a trigonally distorted tetrahedral environment.[2] The trigonal plane contains a Cu ion with a very short Cu−S(Cys) and two typical Cu−N(His) distances. The axial ligand is usually a S(Met) having a long Cu−S bond length, which decreases its donor interaction with the Cu and could be compensated for by the short highly covalent Cu−S(Cys) thiolate bond.[10]

Within the family of blue copper proteins, there are also a number of "perturbed" sites, which exhibit substantially different spectral features than those of the classic blue copper sites.[13,14] The perturbed sites can be divided into two groups based on

[†] Department of Chemistry, Stanford University.
[‡] Stanford Synchrotron Radiation Laboratory, Stanford University.
[§] Occidental College.
[||] University of California, Los Angeles.

(1) Gray, H. B.; Solomon, E. I. In *Copper Proteins*; Spiro, T. G., Ed.; Wiley: New York, 1981; pp 1−39.
(2) Adman, E. T. *Adv. Protein Chem.* **1991**, *42*, 145−197.
(3) Adman, E. T. In *Topics in Molecular and Structural Biology*: *Metalloproteins*; Harrisson, P., Ed.; Macmillan: New York, 1985; Vol. 1, pp 1−42.
(4) Sykes, A. G. **1991**, *107*, 377−408.
(5) Messerschmidt, A. *Struct. Bonding* **1998**, *90*, 37−68.
(6) Randall, D. W.; Gamelin, D. R.; LaCroix, L. B.; Solomon, E. I. *J. Biol. Inorg. Chem.* **2000**, *5*, 16−29.
(7) Nersissian, A. M.; Shipp, E. L. *Adv. Protein Chem.* **2002**, *60*, 271−340.
(8) Penfield, K. W.; Gewirth, A. A.; Solomon, E. I. *J. Am. Chem. Soc.* **1985**, *107*, 4519−4529.
(9) Solomon, E. I.; Baldwin, M. J.; Lowery, M. D. *Chem. Rev.* **1992**, *92*, 521−542.
(10) Guckert, J. A.; Lowery, M. D.; Solomon, E. I. *J. Am. Chem. Soc.* **1995**, *117*, 2817−2844.
(11) Shadle, S. E.; Penner-Hahn, J. E.; Schugar, H. J.; Hedman, B.; Hodgson, K. O.; Solomon, E. I. *J. Am. Chem. Soc.* **1993**, *115*, 767−776.
(12) Lowery, M. D.; Guckert, J. A.; Gebhard, M. S.; Solomon, E. I. *J. Am. Chem. Soc.* **1993**, *115*, 3012−3013.

10.1021/ja035802j CCC: $25.00

structural motifs. The first group includes sites with the same ligand set as plastocyanin (e.g., nitrite reductase[15] and cucumber basic protein[16]); however, the changes in the UV/vis absorption spectrum indicate that the Cu−S(Cys) interaction in the HOMO is rotating from a pure π to a more σ bonding interaction with the thiolate ligand, and MCD spectra indicate a tetragonal distortion of the ligand field relative to that of plastocyanin.[13] The second group includes sites where the chemical nature of the axial ligand is varied; however, the sites remain tetrahedral. This group includes proteins such as stellacyanin, where the axial S(Met) ligand at the Cu of plastocyanin and azurin is replaced by a stronger field O(Gln),[17] and sites in which the S(Met) is replaced with a Leu, Val, or Phe (as in the fungal and plant laccases as well as in tomato plantacyanin),[7,18−20] and hence no axial ligand is provided by the protein.

Understanding how these perturbations affect the electronic and geometric structure of blue copper sites has been the subject of numerous experimental and theoretical studies.[13,14,21−24] In particular, much attention has focused on the role of the axial ligand and how it affects the covalency of the copper−thiolate bond.[13,14,21,22] Spectroscopic evidence indirectly shows that the strength of the axial ligand inversely affects the strength of the Cu−S(thiolate) bond.[14,21,22] However, a direct measurement of the change in Cu−S(Cys) covalency upon substitution of the axial ligand within the same protein scaffold has not yet been made. Here, we focus on spectroscopic studies of wild-type (WT) *Cucumis sativus* stellacyanin and its Q99M and Q99L mutants. This series thus spans the range of classic blue copper sites and the second group of perturbed sites in which the axial ligand is varied from a stronger field O(Gln) to no axial ligand. The covalency of the Cu−S(thiolate) bond is directly probed using S K-edge X-ray absorption spectroscopy (XAS). These data are further supported by Cu K-edge and EXAFS data on the oxidized and reduced forms of the proteins, as well as resonance Raman, absorption, magnetic circular dichroism (MCD), and electron paramagnetic resonance (EPR) spectra. This study provides the unique opportunity to measure the change in the Cu−S(Cys) covalency upon mutation of the axial ligand within the same protein environment, which minimizes contributions from changes in the protein environment (such as dielectric, H-bonding interactions and changes in dipoles). The results are compared to those of the classic blue copper site in azurin. The influence of the axial ligand on the geometric and electronic structure of blue copper sites and its relation to reactivity (i.e., $E°$ and k_{ET}) are discussed.

Finally, it is of interest to note that the blue copper sites in nitrite reductase and cucumber basic protein, which have shorter, stronger axial Cu−S(Met) bonds than does plastocyanin or azurin, undergo a tetragonal distortion. However, stellacyanin, with a strong axial (O)Gln, remains tetrahedral. Previous studies have suggested that in stellacyanin the protein structure limits the Jahn−Teller tetragonal distortion and the site remains distorted tetrahedral.[14] To evaluate the protein contribution to preservation of the tetrahedral structure of stellacyanin, DFT calculations have been performed on the stellacyanin active site with a series of systematically varied constraints.

II. Experimental Section

(A) Sample Preparation and Characterization. WT *C.s.* stellacyanin,[25] its Q99M mutant,[26] and *Pseudomonas aeruginosa* azurin[27] were prepared according to published procedures. The purification procedure of the Q99L mutant was similar to that described previously for WT *C.s.* stellacyanin. Protein concentrations were determined using the extinction coefficient at 280 nm ($\epsilon_{280} = 14\,000\ M^{-1}\ cm^{-1}$ for *C.s.* stellacyanin, Q99M, and Q99L; $\epsilon_{280} = 8440\ M^{-1}\ cm^{-1}$ for *P.a.* azurin). All solutions of WT stellacyanin and the Q99M and Q99L mutants were at pH = 5.5 in 10−30 mM sodium acetate buffer. *P.a.* azurin samples were at pH = 5.1 in 25 mM ammonium acetate buffer. For all S K-edge experiments, the concentrations were 1.9−6.0 mM in protein. Cu K-edge samples were 5.0−6.0 mM in protein and contained ∼40−50% glycerol as a glassing agent. All reduced Cu K-edge samples were prepared by addition of a 10-fold excess of dithionite.

(B) X-ray Absorption Spectroscopy Measurements and Data Analysis. All data were measured at the Stanford Synchrotron Radiation Laboratory under ring conditions of 3.0 GeV and 60−100 mA.

S K-edges. S K-edge data were measured using the 54-pole wiggler beam line 6-2 in high magnetic field mode of 10 kG with a Ni-coated harmonic rejection mirror and fully tuned Si(111) double crystal monochromator. Details of the optimization of this setup for low-energy studies have been described previously.[28] S K-edge measurements were made at ∼4 °C. Protein samples were pre-equilibrated in a water-saturated He atmosphere for ∼0.5−1 h to minimize bubble formation in the sample cell. Protein solutions were loaded via syringe into a Pt-coated Al block sample holder with a 6.35-μm-thick polypropylene window. The data were measured as fluorescence excitation spectra utilizing an ionization chamber as a fluorescence detector.[29,30] All protein samples were monitored for potential effects of photoreduction throughout the course of data collection. WT stellacyanin, the Q99M mutant, and *P.a.* azurin were all oxidized with a 5-fold excess of $K_3[Fe(CN)_6]$, which allowed 10-, 10-, and 8-scan averages, respectively, to be obtained with no indication of photoreduction. For Q99L stellacyanin, a 10-fold excess of $Na_2[IrCl_6]$ was added, which allowed a 6-scan average to be obtained.[31] The energy was calibrated from S K-edge spectra of $Na_2S_2O_3 \cdot 5H_2O$, run at intervals between sample scans.

(13) LaCroix, L. B.; Shadle, S. E.; Wang, Y. N.; Averill, B. A.; Hedman, B.; Hodgson, K. O.; Solomon, E. I. *J. Am. Chem. Soc.* **1996**, *118*, 7755−7768.
(14) LaCroix, L. B.; Randall, D. W.; Nersissian, A. M.; Hoitink, C. W. G.; Canters, G. W.; Valentine, J. S.; Solomon, E. I. *J. Am. Chem. Soc.* **1998**, *120*, 9621−9631.
(15) Adman, E. T.; Godden, J. W.; Turley, S. *J. Biol. Chem.* **1995**, *270*, 27458−27474.
(16) Guss, J. M.; Merritt, E. A.; Phizackerley, R. P.; Freeman, H. C. *J. Mol. Biol.* **1996**, *259*, 686−705.
(17) Hart, P. J.; Nersissian, A. M.; Herrmann, R. G.; Nalbandyan, R. M.; Valentine, J. S.; Eisenberg, D. *Protein Sci.* **1996**, *5*, 2175−2183.
(18) Xu, F.; Shin, W.; Brown, S. H.; Wahleithner, J.; Sundaram, U. M.; Solomon, E. I. *Biochim. Biophys. Acta* **1996**, *1292*, 303−311.
(19) Messerschmidt, A. In *Multicopper Oxidases*; Messerschmidt, A., Ed.; World Scientific: Singapore, 1997; pp 23−80.
(20) Germann, U. A.; Müller, G.; Hunziker, P. E.; Lerch, K. *J. Biol. Chem.* **1988**, *263*, 885−896.
(21) DeBeer, S.; Randall, D. W.; Nersissian, A. M.; Valentine, J. S.; Hedman, B.; Hodgson, K. O.; Solomon, E. I. *J. Phys. Chem. B* **2000**, *104*, 10814−10819.
(22) Palmer, A. E.; Randall, D. W.; Xu, F.; Solomon, E. I. *J. Am. Chem. Soc.* **1999**, *121*, 7138−7149.
(23) Pierloot, K.; DeKerpel, J. O. A.; Ryde, U.; Olsson, M. H. M.; Roos, B. O. *J. Am. Chem. Soc.* **1998**, *120*, 13156−13166.
(24) Ryde, U.; Olsson, M. H. M. *Int. J. Quantum Chem.* **2001**, *81*, 335−347.
(25) Nersissian, A. M.; Mehrabian, Z. B.; Nalbandyan, R. M.; Hart, P. J.; Fraczkiewicz, G.; Czernuszewicz, R. S.; Bender, C. J.; Peisach, J.; Herrmann, R. G.; Valentine, J. S. *Protein Sci.* **1996**, *5*, 2184−2192.
(26) Nersissian, A. M.; Immoos, C.; Hill, M. G.; Hart, P. J.; Williams, G.; Herrmann, R. G.; Valentine, J. S. *Protein Sci.* **1998**, *7*, 1915−1929.
(27) Karlsson, B. G.; Pascher, T.; Nordling, M.; Arvidsson, R. H. A.; Lundberg, L. G. *FEBS Lett.* **1989**, *246*, 211−217.
(28) Hedman, B.; Frank, P.; Gheller, S. F.; Roe, A. L.; Newton, W. E.; Hodgson, K. O. *J. Am. Chem. Soc.* **1988**, *110*, 3798−3805.
(29) Lytle, F. W.; Greegor, R. B.; Sandstrom, D. R.; Marques, E. C.; Wong, J.; Spiro, C. L.; Huffman, G. P.; Huggins, F. E. *Nucl. Instrum. Methods* **1984**, *226*, 542−548.
(30) Stern, E. A.; Heald, S. M. *Rev. Sci. Instrum.* **1979**, *50*, 1579−1582.

(31) It should be noted that all samples were run both before and after the addition of excess oxidant. For all samples, the S K-edge data remained very similar, except for an increase in the pre-edge intensity of Q99L stellacyanin, consistent with the presence of some reduced copper. Similarly,

The maximum of the first pre-edge feature in the spectrum was fixed at 2472.02 eV. A step size of 0.08 eV was used over the edge region. Data were averaged, and a smooth background was removed from all spectra by fitting a polynomial to the pre-edge region and subtracting this polynomial from the entire spectrum. Normalization of the data was accomplished by fitting a flattened polynomial or straight line to the post-edge region and normalizing the edge jump to 1.0 at 2490 eV. Fits to the edges were performed using the program EDG_FIT.[32] Second derivative spectra were used as guides to determine the number and position of peaks. Pre-edge and rising edge features were modeled by pseudo-Voigt line shapes. For the pre-edge feature, a fixed 1:1 ratio of Lorentzian to Gaussian contributions was used. Fits were performed over several energy ranges. The reported intensity values and standard deviations are based on the average of all good fits. Normalization procedures can introduce ~3% error in the total pre-edge peak areas, in addition to the error resulting from the fitting procedure. The reported covalencies are based on using plastocyanin as a reference, for which 1.02 intensity units corresponds to 38% S 3p character in the Cu−S(Cys) bond.

Cu K-edges and EXAFS. Cu K-edge data were measured on unfocused 8-pole wiggler beam line 7-3 using a Si(220) monochromator for energy selection. The monochromator was detuned 50% to minimize higher harmonic components in the X-ray beam. Samples were loaded into 1-mm Lucite XAS cells with 63.5-μm Mylar windows and then frozen immediately by immersion in liquid nitrogen prior to data collection. The samples were maintained at 10 K during the data collection using an Oxford Instruments CF1208 continuous flow liquid helium cryostat. Data were measured in fluorescence mode using either a Canberra Ge 18-element array detector (for concentrations < 5 mM) or an Ar-filled ionization chamber[29,30] detector equipped with a Ni filter and Soller slits (for concentrations > 5 mM). XAS data were measured to $k = 13.4$ Å^{-1} (the zinc K-edge), as all samples were found to contain a small amount of zinc. Data for three separate preparations of oxidized and two preparations of reduced Q99L stellacyanin were obtained; however, in all cases the data have been truncated beyond $k = 11$ Å^{-1} due to contributions from ice diffraction at high k resulting from a poor glass. Internal energy calibration was performed by simultaneous measurement of the absorption of a Cu foil placed between a second and third ionization chamber. The first inflection point of the Cu foil was assigned to 8980.3 eV. All oxidized samples were monitored for photoreduction throughout the course of data collection. For the Q99M and Q99L mutants, a 3−5-fold excess of $K_3[Fe(CN_6)]$ and $Na_2[IrCl_6]$, respectively, was added to help minimize the effect of photoreduction. Only those scans which showed no evidence of photoreduction were used for edge comparisons. For the EXAFS analysis, only scans which showed less than 5% photoreduction (14 scans for *C.s.* stellacyanin, 12 scans for Q99M stellacyanin, and 14 scans for Q99L stellacyanin) were averaged.

The averaged data were processed as described previously[33] by fitting a second-order polynomial to the postedge region and subtracting this background from the entire spectrum. A three-region cubic spline was used to model the smooth background above the edge. Normalization of the data was achieved by subtracting the spline and normalizing the edge jump to 1.0 at 9000 eV. The resultant EXAFS was k^3-weighted to enhance the impact of high-k data. The edges of Cu(I) stellacyanin and its mutants were analyzed as described previously.[34]

Theoretical EXAFS signals $\chi(k)$ were calculated using FEFF (version 6.0)[35,36] and fit to the data using EXAFSPAK.[37] The experimental energy threshold, E_0 (the point at which $k = 0$), was chosen as 8990 eV. The structural parameters that varied during the refinements were the bond distance (R) and the bond variance (σ^2). The σ^2 is related to the Debye−Waller factor, which is a measure of thermal vibration and static disorder of the absorbers/scatterers. Coordination numbers were systematically varied in the course of the analysis, but they were not allowed to vary within a given fit. Single scattering paths and the corresponding multiple scattering paths were linked during the course of refinements.

(C) Resonance Raman. Resonance Raman spectra were collected with a Princeton Instruments ST-135 back-illuminated CCD detector on a Spex 1877 CP triple monochromator with 1200, 1800, and 2400 grooves/mm holographic spectrograph gratings. Continuous wave coherent Kr ion (Innova90C-K) and an Ar ion (Sabre-25/7) visible and UV laser lines were used as variable excitation sources. A polarization scrambler was used between the sample and the spectrometer. The Raman energy was calibrated with Na_2SO_4. Frequencies are accurate to within <2 cm^{-1}. Samples were loaded in 4 mm NMR tubes and stored in liquid nitrogen.

(D) Absorption and MCD. Room-temperature UV/visible absorption spectra were obtained using a Hewlett-Packard HP8452A diode array spectrophotometer in either 1.0, 0.2, or 0.1 cm quartz cuvettes. Low-temperature magnetic circular dichroism spectra were obtained using two Jasco spectropolarimeters. Each is equipped with a modified sample compartment to accommodate focusing optics and an Oxford Instruments SM4000-7T superconducting magnet/cryostat. This arrangement allows data collection at temperatures from 1.6 to 290 K and field up to 7 T.[38] A Jasco J810 spectropolarimeter operating with a S-20 photo multiplier tube was used to access the visible and ultraviolet spectral region. A Jasco J200 spectropolarimeter operating with a liquid nitrogen cooled InSb detector was used for the near-infrared region. Depolarization of the light by the MCD samples was monitored by the effect the sample had on the circular dichroism of nickel (+)-tartarate placed before and after the sample.[39] In all cases, the depolarization was less than 5%. MCD samples were run in cells fitted with quartz disks and a 0.3 cm rubber gasket spacer. Simultaneous Gaussian fitting of the absorption and MCD spectra was performed using the Peak-Fit program (Jandel).

(E) EPR and Copper Quantitation. EPR spectra were obtained using a Bruker ER083CS spectrometer. Sample temperatures were maintained at 77 K using a liquid N_2 finger dewar. For WT stellacyanin, Q99M stellacyanin, and azurin S K-edge samples, the concentration of paramagnetic copper was determined from spin quantitation of EPR spectra with a 1 mM aqueous copper standard run in the same tube as the sample.[40] For these samples, a total spin of (0.97−1.00) ± 0.05 was obtained. The blue copper site in the Q99L mutant appeared to be unstable, which was manifested by the presence of a variable amount of tightly bound copper with Type 2 features in addition to the Type 1 Cu site. Although it complicated copper quantitation, the Q99L samples used for Cu K-edge XAS experiments were estimated to contain an ~1:1 ratio of Type 2 to Type 1 Cu(II), based on EPR simulations. However, Q99L samples used for S K-edge XAS quantitation showed only a T1 copper EPR signal. These samples were used for the EPR data and simulations presented in this paper. Simulation

the overall Cu K-edge shape remained very similar after addition of oxidant, except for the decreased intensity of a feature at ~8983 eV in Q99L corresponding to the presence of some reduced copper. EPR spectra before and after the addition of oxidant gave equivalent parameters.

(32) George, G. N. *EDG_FIT*; Stanford Synchrotron Radiation Laboratory, Stanford Linear Accelerator Center, Stanford University, Stanford, CA 94309.
(33) DeWitt, J. G.; Bentsen, J. G.; Rosenzweig, A. C.; Hedman, B.; Green, J.; Pilkington, S.; Papaefthymiou, G. C.; Dalton, H.; Hodgson, K. O.; Lippard, S. J. *J. Am. Chem. Soc.* **1991**, *113*, 9219−9235.
(34) Kau, L.-S.; Spira-Solomon, D. J.; Penner-Hahn, J. E.; Hodgson, K. O.; Solomon, E. I. *J. Am. Chem. Soc.* **1987**, *109*, 6433−6442.
(35) Rehr, J. J.; Mustre de Leon, J.; Zabinsky, S. I.; Albers, R. C. *J. Am. Chem. Soc.* **1991**, *113*, 5135−5140.
(36) Mustre de Leon, J.; Rehr, J. J.; Zabinsky, S. I.; Albers, R. C. *Phys. Rev. B* **1991**, *44*, 4146−4156.
(37) George, G. N. *EXAFSPAK*; Stanford Synchrotron Radiation Laboratory, Stanford Linear Accelerator Center, Stanford University, Stanford, CA 94309.
(38) Allendorf, M. D.; Spira, D. J.; Solomon, E. I. *Proc. Natl. Acad. Sci. U.S.A.* **1985**, *82*, 3063−3067.
(39) Browett, W. R.; Fucaloro, A. F.; Morgan, T. V.; Stephens, P. J. *J. Am. Chem. Soc.* **1983**, *105*, 1868−1872.
(40) Carithers, R. P.; Palmer, G. J. *J. Biol. Chem.* **1981**, *256*, 7967−7976.

of the Type 1/Type 2 mixed sample gave equivalent parameters for the T1 site. The Q99L mutant could not be spin quantitated by EPR because a strong oxidant (Na_2IrCl_6) needed to be added to it to completely oxidize the Type 1 sites. The oxidant is paramagnetic, thus contributing to the background signal and introducing significant error to the spin quantitation. Hence, the total copper concentration for Q99L stellacyanin was determined spectrophotometrically using the 2,2′-biquinoline assay,[41] which indicated the protein was 95 ± 3% loaded with copper.

(F) Density Functional Calculations. Gradient corrected density functional calculations (GGA-DFT) were carried out using the Gaussian98[42] package on a 50-cpu heterogeneous cluster of SGI and IBM PC compatible computers. The Becke88[43] exchange and Perdew86[44] correlation nonlocal functionals were used with Wosko−Vilk−Nussair local functionals[45] as implemented in the software package (BP86). The triple- (VTZ*)[46] and double-ζ (6-31G*)[47] Gaussian type all-electron basis sets (BS5) were employed with polarization functions for the metal and ligands, respectively. This basis set has been previously shown to be theoretically converged for Cu^{II}-containing systems, and additional polarization or diffuse functions do not improve the electronic structure description.[48] Because the standard GGA-DFT calculations give too much ligand character in the ground-state wave function as compared to experimental values, 38% of total DF exchange was replaced with HF exchange (B(38HF)P86), giving an accurate bonding description as discussed for other cupric systems.[48c] Population analyses were performed by means of Weinhold's natural population analysis (NPA)[49] including the Cu 4p orbitals into the valence set (NPA(4p)).

The active site models were constructed from imidazole, methyl thiolate, and propionic amide molecules. The atomic coordinates of the active site were taken from the 1.6-Å resolution X-ray crystal structure of cucumber stellacyanin (PDB code 1JER[17]).

Geometry optimizations were performed with frequent updates of the force constants to stay as close as possible to the lowest energy pathway. Stationary points were restarted with continuous updates of force constants until optimization stopped due to negligible forces. In all optimizations, the GDIIS[50] optimizer was applied due to the flat potential energy surface of the Cu site.

III. Results and Analysis

(A) S K-edges. A comparison of the normalized S K-edge spectra for WT, Q99M, and Q99L stellacyanin is shown in Figure 1a. The renormalized spectra (Figure 1b) account for the fact that a different number of sulfur atoms contribute to the pre-edge and edge features and also adjust for differences in T1 Cu(II) loading (see Experimental Section).[51] The renormalized spectra show different pre-edge intensities, with WT

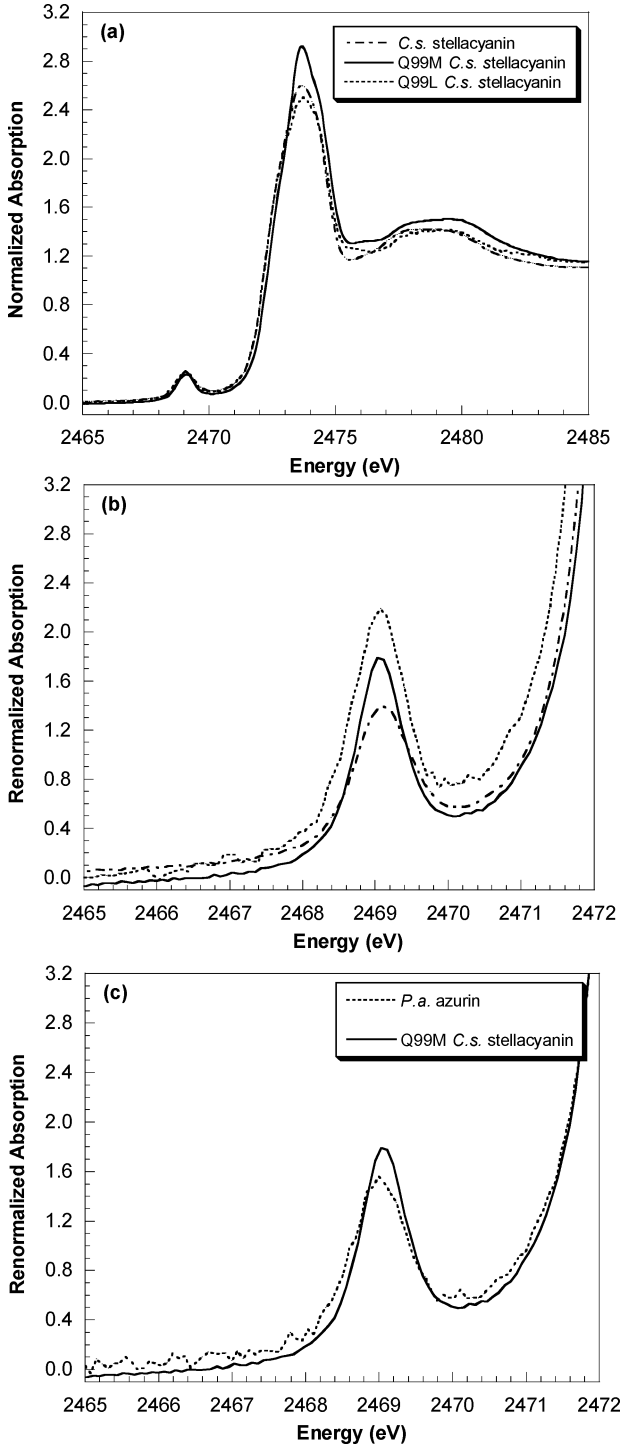

Figure 1. (a) Comparison of the normalized S K-edge spectra of oxidized WT, Q99M, and Q99L stellacyanins. (b) The renormalized pre-edge data (expanded scale) of the samples shown in (a). (c) Comparison of the renormalized S K-edge spectra of oxidized Q99M stellacyanin and azurin.

(41) Felsenfeld, G. *Arch. Biochem. Biophys.* **1960**, *87*, 247−251.
(42) Frisch, M. J.; Trucks, G. W.; Schlegel, H. B.; Scuseria, G. E.; Robb, M. A.; Cheeseman, J. R.; Zakrzewski, V. G.; Montgomery, J. A. J.; Stratmann, R. E.; Burant, J. C.; Dapprich, S.; Millam, J. M.; Daniels, A. D.; Kudin, K. N.; Strain, M. C.; Farkas, O.; Tomasi, J.; Barone, V.; Cossi, M.; Cammi, R.; Mennucci, B.; Pomelli, C.; Adamo, C.; Clifford, S.; Ochterski, J.; Petersson, G. A.; Ayala, P. Y.; Cui, Q.; Morokuma, K.; Malick, D. K.; Rabuck, A. D.; Raghavachari, K.; Foresman, J. B.; Cioslowski, J.; Ortiz, J. V.; Stefanov, B. B.; Liu, G.; Liashenko, A.; Piskorz, P.; Komaromi, I.; Gomperts, R.; Martin, R. L.; Fox, D. J.; Keith, T.; Al-Laham, M. A.; Peng, C. Y.; Nanayakkara, A.; Gonzalez, C.; Challacombe, M.; Gill, P. M. W.; Johnson, B.; Chen, W.; Wong, M. W.; Andres, J. L.; Head-Gordon, M.; Replogle, E. S.; Pople, J. A. *Gaussian 98*, revision A.11; Gaussian, Inc.: Pittsburgh, PA, 1998.
(43) Becke, A. D. *Phys. Rev. A*: *Gen. Phys.* **1988**, *38*, 3098−3100.
(44) Perdew, J. P. *Phys. Rev. B*: *Condens. Mater.* **1986**, *33*, 8822−8824.
(45) Vosko, S. H.; Wilk, L.; Nusair, M. *Can. J. Phys.* **1980**, *58*, 1200−1211.
(46) Schaefer, A.; Horn, H.; Ahlrichs, R. *J. Chem. Phys.* **1992**, *97*, 2571−2577.
(47) (a) Hariharan, P. C.; Pople, J. A. *Theor. Chim. Acta* **1973**, *28*, 213−222. (b) Francl, M. M.; Pietro, W. J.; Hehre, W. J.; Binkley, J. S.; Gordon, M. S.; DeFrees, D. J.; Pople, J. A. *J. Chem. Phys.* **1982**, *77*, 3654−3665. (c) Rassolov, V. A.; Pople, J. A.; Ratner, M. A.; Windus, T. L. *J. Chem. Phys.* **1998**, *109*, 1223−1229.
(48) (a) Siegbahn, P. E. M.; Blomberg, M. R. A. *Chem. Rev.* **2000**, *100*, 421−437. (b) Ryde, U.; Olsson, M. H. M.; Pierloot, K. *Theor. Comput. Chem.* **2001**, *9*, 1−55. (c) Szilagyi, R. K.; Metz, M.; Solomon, E. I. *J. Phys. Chem. A* **2002**, *106*, 2994−3007.
(49) (a) Foster, J. P.; Weinhold, F. *J. Am. Chem. Soc.* **1980**, *102*, 7211−7218. (b) Reed, A. E.; Curtiss, L. A.; Weinhold, F. *Chem. Rev.* **1988**, *88*, 899−926. (c) Carpenter, J. E.; Weinhold, F. *J. Mol. Struct.* (*THEOCHEM*) **1988**, *169*, 41−62.
(50) (a) Csaszar, P.; Pulay, P. *J. Mol. Struct.* (*THEOCHEM*) **1984**, *114*, 31−34. (b) Farkas, O.; Schlegel, H. B. *J. Chem. Phys.* **1998**, *109*, 7100−7104. (c) Farkas, O.; Schlegel, H. B. *J. Chem. Phys.* **1999**, *111*, 10806−10814.

(51) There are 6 sulfurs (3 Met and 3 Cys) in WT stellacyanin, 7 sulfurs (4 Met and 3 Cys) in the Q99M mutant, 6 sulfurs (3 Met and 3 Cys) in the Q99L mutant, and 9 sulfurs (3 Cys and 6 Met) in azurin. For all four proteins, all of the sulfurs will contribute to the edge, while only one Cys thiolate contributes to the pre-edge.

Table 1. Fit Results for S K-edge XAS Data

compound	pre-edge energy (eV)[a]	renormalized pre-edge intensity[b]	%S covalency[b,c]
C.s. stellacyanin	2469.1	1.11	41 ± 4
Q99M *C.s.* stellacyanin	2469.1	1.26	47 ± 4
Q99L *C.s.* stellacyanin	2469.0	1.47	54 ± 6
P.a. azurin	2469.0	1.21	45 ± 3
plastocyanin[d]	2469.0	1.02	38

[a] Energies reported are within an error of ±0.1 eV. [b] The %S covalency has been renormalized to account for the different number of sulfurs which contribute to the pre-edge and edge features and also to account for differences in oxidized T1 copper loading. [c] Error reported is the standard deviation of all good fits; an additional 3% error is introduced by the normalization procedure. [d] Reference 11.

stellacyanin being the least intense, followed by the Q99M mutant, and then the Q99L mutant (Table 1). The differences in pre-edge intensities indicate different sulfur covalencies in the WT and mutant proteins. When plastocyanin was used as a reference,[11] these values are 41%, 47%, and 54% (Table 1) for WT, Q99M, and Q99L stellacyanins, respectively.[52] These results demonstrate that weakening the axial ligand (based on MCD results, vide infra) increases the covalency of the Cu−S(thiolate) bond.

A comparison of the renormalized S K-edge spectra of azurin and Q99M stellacyanin is shown in Figure 1c. These data indicate that azurin has a similar pre-edge intensity (Figure 1c and Table 1) and hence a covalency close to that for Q99M stellacyanin (45% for azurin vs 47% for Q99M stellacyanin). This could be attributed to the similar ligand environment (N_2-(His)S(Cys)S(Met)) in these two proteins.[53,54] All four proteins exhibit the same pre-edge maximum energy (within error) at ~2469 eV (Table 1). For azurin and Q99M, this is expected, as both the ligand-field splitting of the d-manifold (vide infra) and the effective nuclear charge (Z_{eff}) on the metal center are the same. On going from WT to Q99M to Q99L stellacyanin, the average ligand-field transition energy increases (based on MCD results vide infra), which would tend to increase the energy of the pre-edge transition. However, the fact that there is no change in pre-edge energy indicates that the ligand-field contribution is countered by the increase in effective nuclear charge on the Cu as the axial ligand is weakened across this series (consistent with EPR analysis, vide infra). It is important to note that the increase in S 3p character across this series indicates that the S 1s core should also shift to deeper binding energy on going from WT to Q99M to Q99L. Thus, the similarity in the pre-edge transition energies requires that the change in Z_{eff} is at least as great as the change in ligand field and is likely somewhat greater to also compensate for the S 1s core shift. (This cannot be extracted directly from the XAS data as the S K-edge also has contributions from the other noncoordinating sulfurs in the protein.)

(52) The shifts in rising edge background are attributed to both a different total number of sulfurs in the proteins and to differences in copper loading. Fits to the pre-edge region account for the differences in the rising edge background.

(53) It should be noted that both Q99M stellacyanin and azurin have an apparent higher covalency value than plastocyanin.[11] All Q99M stellacyanin and azurin samples were fully oxidized and spin quantitated to determine copper loading; thus, these data most likely reflect a more accurate covalency estimate for a classic blue copper site.

(54) It should be noted that for azurin a distant (~3 Å) Cu−O interaction to a backbone amide carbonyl, trans to the thioether, is sometime discussed, which is not present in the Q99M mutant. However, at this distance, little covalent bonding interaction is present between the Cu and the compact O 2p orbitals, ref 6.

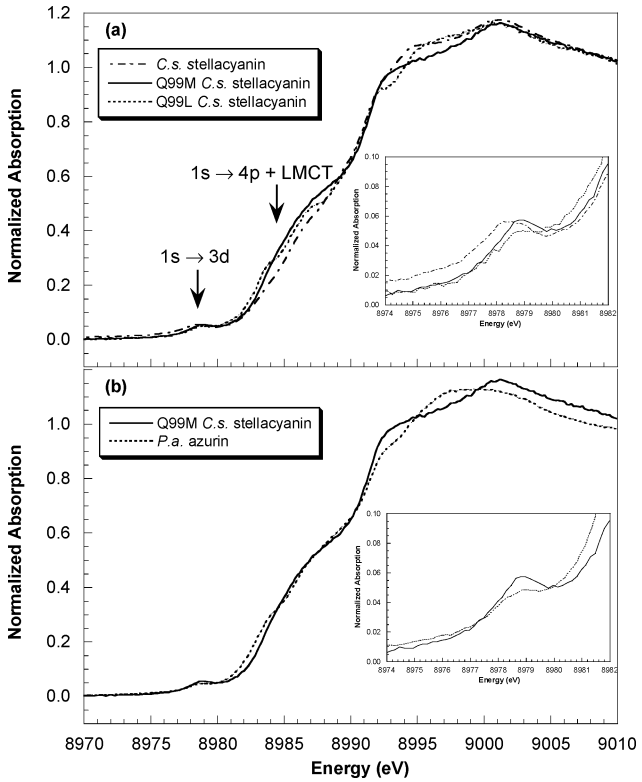

Figure 2. (a) Comparison of the normalized Cu K-edge spectra of oxidized WT, Q99M, and Q99L stellacyanins. Arrows mark the 1s → 3d and 1s → 4p + LMCT transitions. (b) Comparison of the normalized Cu K-edge spectra of oxidized Q99M stellacyanin and azurin. Insets show expanded pre-edge regions.

(B) Cu(II) K-edges and EXAFS. Edges. A comparison of the Cu K-edge spectra of the oxidized forms of WT, Q99M, and Q99L stellacyanin is shown in Figure 2a. The spectra are all characteristic of Cu(II); however, differences are evident in the pre-edge region (~8979 eV, inset in Figure 2a) and on the rising edge (~8984−8987 eV).

All three proteins exhibit a weak pre-edge feature at ~8979 eV (Figure 2a, inset), which corresponds to a Cu 1s → 3d transition. For Q99M stellacyanin, the pre-edge feature is shifted ~0.5 eV to higher energy than for WT stellacyanin. This may be attributed to both the increase in the ligand field of the Q99M mutant relative to WT stellacyanin (by ~0.1 eV based on the average energy of the MCD d → d bands, vide infra) and to the increase in Z_{eff} on the copper due to a weaker ligand donor set. This is consistent with the shifts that are observed on going from stellacyanin to the classic blue copper sites in azurin and plastocyanin[21] and indicates that the O(Gln) interaction in WT stellacyanin is stronger than the S(Met) interaction in both the classic blue copper sites and the Q99M mutant of stellacyanin. For Q99L stellacyanin, interpretation of the pre-edge energy is complicated by the presence of an additional Cu(II) which also contributes to the pre-edge region and prevents accurate determination of the T1 Q99L stellacyanin pre-edge energy.

The transition at ~8984 eV has been previously assigned as a 1s → 4p transition with concurrent ligand-to-metal charge transfer, which gains intensity through final state relaxation (i.e., formally a two-electron shakedown transition).[34,55,56] On going

(55) Kosugi, N.; Yokoyama, T.; Asakura, K.; Kuroda, H. *Chem. Phys.* **1984**, *91*, 249−256.

(56) Bair, R. A.; Goddard, W. A., III. *Phys. Rev. B* **1980**, *22*, 2767−2776.

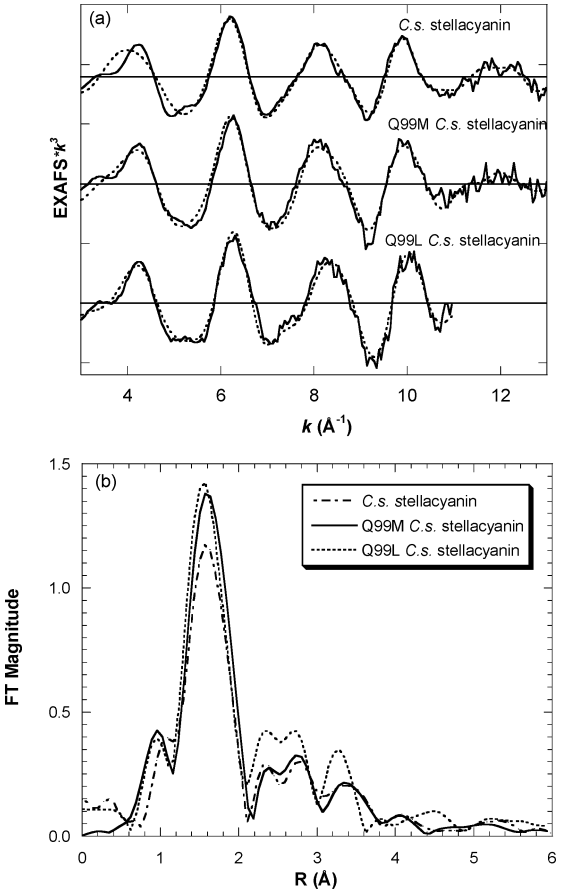

Figure 3. (a) Experimental EXAFS data (—) and fits to the data (- - -) for oxidized WT, Q99M, and Q99L stellacyanins (each major tick on the ordinate scale represents 5 units) and (b) nonphase shift corrected Fourier transforms.

from WT to Q99M stellacyanin, the intensity of the shakedown feature increases. On the basis of a previous VBCI analysis applied to the Cu K-edges of plastocyanin and stellacyanin, this reflects more covalent thiolate−Cu(II) bonding in Q99M stellacyanin than in the WT.[21] For Q99L stellacyanin, the shakedown region is again complicated by the presence of an additional Cu(II) with Type 2 features (see Experimental Section), which prevents an accurate assessment of the intensities in this region. However, there is clearly more intensity at lower energy, consistent with a highly covalent Cu(II)−S(Cys) bond (which cannot be due to adventitious Cu(II)).[57]

A comparison of the Cu K-edge of Q99M stellacyanin to that of the classic blue copper site in azurin is shown in Figure 2b. Q99M stellacyanin and azurin have very similar pre-edge energies and similar shakedown intensities, indicating that these two sites, both with an axial methionine, have similar electronic properties. It should be noted, however, that there is a small difference in the pre-edge intensities of these two proteins, which may reflect small differences in 4p mixing into the d-manifold.[11]

EXAFS. The k^3-weighted EXAFS data and fits for the oxidized forms of WT, Q99M, and Q99L stellacyanins are shown in Figure 3a. A comparison of the corresponding Fourier transforms (FTs; $k = 2-11$ Å^{-1}) is shown in Figure 3b. The EXAFS signals of the three proteins are generally similar with slight changes in the frequency on going from WT to Q99M to Q99L stellacyanin. There are also subtle changes in the FTs of these proteins. In particular, the first shell FT amplitude for Q99M is higher than that of the WT, likely resulting from a slightly different distribution of the first shell σ^2 values (Table 2). In addition, the FT amplitude of Q99L is shifted to a slightly lower *R*-value, indicating a somewhat shorter average first shell distance (Table 2). These differences, as they relate to the fit results, are considered below.

Fits to oxidized WT stellacyanin were previously reported in ref 21. FEFF-based fits from Q99M and Q99L stellacyanin were performed using the 1.6-Å crystal structure of oxidized *C.s.* stellacyanin[17] as a starting model and modifying the axial ligand identity and distance. WT stellacyanin was best fit by including 1 Cu−S at 2.17 Å and 2 Cu−N interactions at 1.96 Å. Very similar fit results were obtained for Q99M stellacyanin (Table 2), with 1 Cu−S at 2.16 Å and 2 Cu−N at 1.95 Å. For Q99L stellacyanin, the best fit was obtained by inclusion of 1 Cu−S at 2.13 Å and 2 Cu−N at 1.94 Å.[58] On the basis of the results of EPR simulations, the data were also modeled as a 50:50 mixture of the Q99L T1 site (i.e., 1 Cu−S and 2 Cu−N) and the exogenous normal Cu(II) site (i.e., 4 Cu−N/O). This resulted in a visually similar fit (with 0.5 Cu−S at 2.12 Å and 3 Cu−N at 1.94 Å; Table 2, Q99L stellacyanin fit 2); however, the error value is slightly increased, and the σ^2 value for the Cu−S interaction is unreasonably low. This may indicate that the fit does not model the exogenous Cu(II) site well. However, it should be emphasized that the Cu−S and Cu−N distances remain unchanged (within error) whether the data are modeled as a single species or as a mixture. In all cases, multiple scattering interactions from the imidazole rings of the ligating histidines were necessary to fit the outer shells. Fit results showed no evidence for the axial S(Met), which on the basis of similar blue copper sites is expected to be distant (>2.8 Å)[59,60] and weakly interacting, and therefore would not be expected to contribute significantly to the EXAFS signal. Fit results also showed no evidence for the axial leucine, which is expected as it cannot coordinate to the copper. In addition, it should be noted that the EXAFS data showed no evidence for the axial O(Gln) in WT stellacyanin;[21] however, the Cu(II) edge data clearly indicate a stronger axial interaction in WT stellacyanin than in the Q99M mutant (vide supra).

A comparison of the EXAFS fit results for the oxidized forms of WT, Q99M, and Q99L stellacyanin shows that the changes at the copper site are limited but reproducible. The Cu−N(His) distances are all within a 0.02 Å range of each other, while the Cu−S(Cys) bond is decreased by ∼0.04−0.05 Å across the series. Within the error limits of EXAFS, the changes are small;[61] however, the trend is consistent with the S K-edge

(57) On the basis of the EPR parameters, the additional tightly bound Cu(II) site is significantly less covalent than a T1 copper site and thus should have a much less intense shakedown feature. Hence, it is likely that the shakedown feature for the Q99L T1 site is even more intense than that of Q99M. This trend is consistent with S K-edge results. It should also be noted that the feature at ∼8983 eV in the Q99L Cu K-edge spectrum corresponds to the presence of a small amount of reduced copper.

(58) The Cu K-edge data indicate a small amount of Cu(I) in oxidized Q99L stellacyanin. This would have only a small effect on the Cu−S distance of Q99L and would if anything make the Cu−S distance slightly longer.

(59) Guss, J. M.; Bartunik, H. D.; Freeman, H. C. *Acta Crystallogr.* **1992**, *B48*, 790−811.

(60) Nar, H.; Messerschmidt, A.; Canters, G. W. *J. Mol. Biol.* **1991**, *221*, 765−772.

(61) The error in first shell bond lengths is ∼0.02 Å. Data for WT and Q99M stellacyanin were fit over the full data range ($k = 2-13.4$ Å^{-1}) and over a truncated data range ($k = 2-11$ Å^{-1}) for comparison to Q99L stellacyanin fits. Fits over the shorter data range did not change the Cu−S or Cu−N distances.

Table 2. A Comparison of EXAFS Fit Results for WT Stellacyanin and the Q99M and Q99L Mutants

	C.s. stellacyanin			Q99M *C.s.* stellacyanin			Q99L *C.s.* stellacyanin (fit 1)			Q99L *C.s.* stellacyanin (fit 2)[a]		
	CN	*R* (Å)	σ^2 (Å^2)	CN	*R* (Å)	σ^2 (Å^2)	CN	*R* (Å)	σ^2 (Å^2)	CN	*R* (Å)	σ^2 (Å^2)
						Oxidized						
Cu−N	2	1.96	0.0026	2	1.95	0.0010	2	1.94	0.0012	3	1.94	0.0038
Cu−S	1	2.17	0.0042	1	2.16	0.0016	1	2.13	0.0033	0.5	2.12	0.0008
Cu−C2/C5[b]	4	2.96	0.0044	4	2.95	0.0045	4	2.94	0.0015	4	2.94	0.0017
Cu−N−C2/C5	4	3.08	0.0044	4	3.12	0.0045	4	3.11	0.0015	4	3.12	0.0017
Cu−C3/N4[b]	4	3.92	0.0043	4	3.90	0.0091	4	3.83	0.0079	4	3.85	0.0078
Cu−N−C3/N4	4	4.23	0.0043	4	4.17	0.0092	4	4.10	0.0087	4	4.09	0.0087
normalized error[c]			0.277			0.331			0.364			0.395
						Reduced						
Cu−N	2	2.02	0.0015	2	2.02	0.0013	2	2.02	0.0027	3	2.00	0.0027
Cu−S	1	2.22	0.0016	1	2.22	0.0017	1	2.22	0.0019	0.5	2.21	0.0019
Cu−C2/C5[b]	4	3.03	0.0065	4	3.04	0.0061	4	3.01	0.0063	4	3.01	0.0072
Cu−N−C2/C5	4	3.14	0.0066	4	3.18	0.0061	4	3.14	0.0063	4	3.14	0.0063
Cu−C3/N4[b]	4	4.26	0.0052	4	4.25	0.0051	4	4.28	0.0033	4	4.27	0.0028
Cu−N−C3/N4	4	4.34	0.0052	4	4.32	0.0051	4	4.38	0.0039	4	4.37	0.0033
normalized error[c]			0.259			0.384			0.198			0.214

[a] These fits assume a 50:50 mixture of the Q99L T1 site and the additional tightly bound copper site. [b] These components represent a single scattering path (top) and the corresponding multiple scattering path (line below). [c] Error is given by $\sum[(\chi_{obsd} - \chi_{calcd})^2k^6]/\sum[(\chi_{obsd}^2k^6]$.

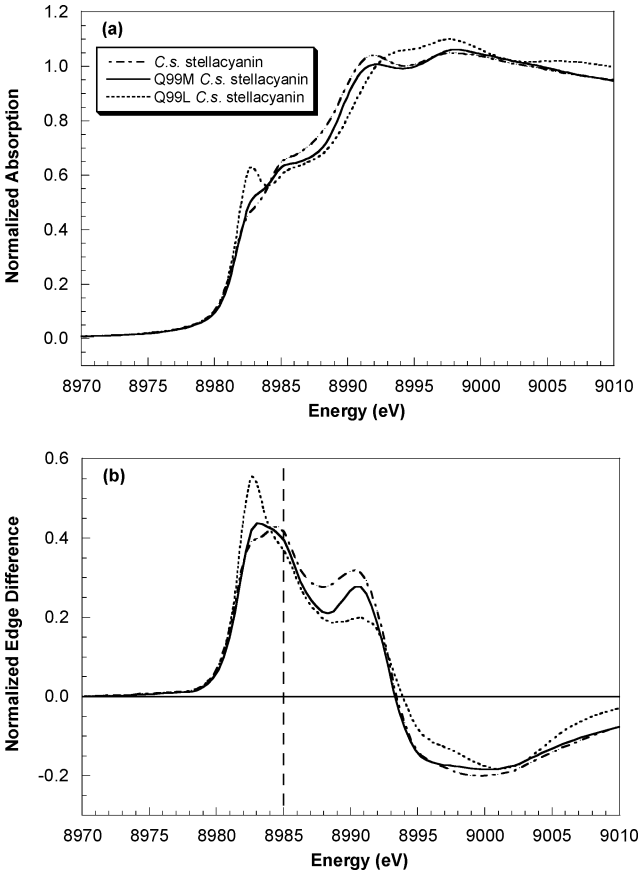

Figure 4. (a) Cu K-edge data and (b) the normalized edge difference spectra for reduced WT, Q99M, and Q99L stellacyanins.

results (vide supra) and parallels the trend observed in resonance Raman spectroscopy (vide infra).

(C) Cu(I) K-edges and EXAFS. Edges. A comparison of the Cu K-edges of the reduced forms of WT, Q99M, and Q99L stellacyanin and the corresponding edge difference spectra are shown in Figure 4. For all three proteins, there is a distinct shoulder at ~8984 eV that is characteristic of Cu(I). The intensity of this feature is dependent on the ligand-field splitting of the Cu 4p orbitals and thus reflects changes in the active-site coordination environment.[34] As the coordination number decreases, the intensity of this feature increases. On going from WT to Q99M to Q99L stellacyanin, the intensity of this feature increases, indicating a decrease in coordination number, which likely reflects the weakened axial interaction across this series.[62] This indicates that it is unlikely that an exogenous ligand is binding in the axial position of the Q99M or Q99L Cu sites and also shows that the same axial ligand strength trend is observed for Cu(I) as for Cu(II).

EXAFS. The k^3-weighted EXAFS data and fits for the reduced forms of WT, Q99M, and Q99L stellacyanins are shown in Figure 5a, and the corresponding FTs ($k = 2-11$ Å^{-1}) are shown in Figure 5b. As was the case for the oxidized protein, the overall EXAFS signals of the three reduced proteins are generally very similar with only slight changes in the frequency across the series. The changes in the FTs of these proteins are also very small, with a slight decrease in the average first shell position on going from WT to Q99M to Q99L stellacyanin. In all three proteins, the outer shell is comprised of multiple scattering interactions from the ligating imidazoles of the histidines. FEFF-based fits were performed using comparable models as for the oxidized proteins. In all cases, the data were best fit by 1 Cu−S at 2.02 Å and 2 Cu−N at 2.22 Å (Table 2). Q99L stellacyanin could also be fit as a mixture of the Q99L T1 site (i.e., 2 Cu−N and 1 Cu−S) and the additional tightly bound Cu site (i.e., 4 Cu−N/O), with 3 Cu−N at 2.00 Å and 0.5 Cu−S at 2.21 Å (Table 2, Q99L stellacyanin, Fit 2). The fit was visually similar; however, the fit error increased slightly. As was the case for the oxidized proteins, fit results showed no evidence for a contribution from the axial ligands. In contrast to the oxidized proteins, the reduced proteins show no change in the Cu−S distances (outside of the ±0.02 Å error limit) across the series.

(D) Resonance Raman. Figure 6 presents the resonance Raman spectra of WT *C.s.* Stellacyanin and its Q99M and Q99L mutants. All spectra were obtained with excitation at 647.1 nm into the S(Cys) → Cu charge-transfer band. As for other blue copper proteins, the spectra are characterized by a complex

(62) It should be noted that the presence of an additional tightly bound four-coordinate copper in Q99L stellacyanin would tend to decrease the intensity of the ~8984 eV feature, and thus the intensity of this feature should be even greater.

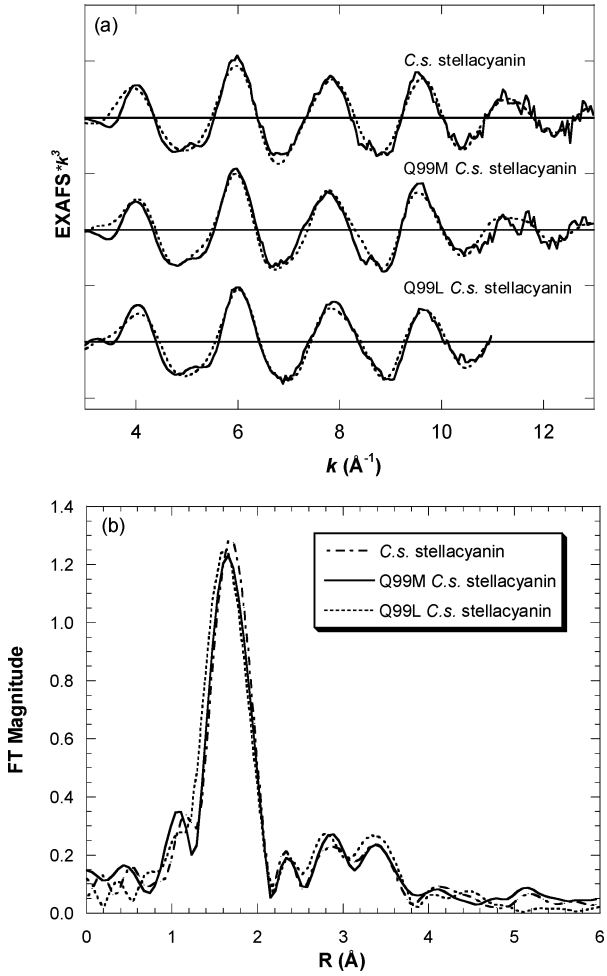

Figure 5. (a) Experimental EXAFS data (—) and fits to the data (- - -) for reduced WT, Q99M, and Q99L stellacyanins (each major tick on the ordinate scale represents 5 units) and (b) nonphase shift corrected Fourier transforms.

envelope of vibrations centered at ~400 cm^{-1},[63] all of which have some Cu−S character. The intensity weighted average, $\langle \nu_{Cu-S} \rangle$, of these peaks can be used as an indicator of the Cu−S bond strength.[64] The following values of $\langle \nu_{Cu-S} \rangle$ were obtained: 386 cm^{-1} (WT), 393 cm^{-1} (Q99M), and 417 cm^{-1} (Q99L).

The variation in stretching force constant is often described using Badger's rule:[65]

$$k = 1.86(r_e - d_{ij})^{-3} \quad (1)$$

where r_e is the equilibrium bond length, and the constant d_{ij} is fixed for bonds between atoms of rows i and j of the periodic table. The stretching frequency for the mutants is estimated using the Cu−S(Cys) bond distances as obtained from EXAFS (2.17 Å in WT, 2.16 Å in Q99M, and 2.13 Å in Q99L). When WT is used as a reference, the calculated values for Q99M (396 cm^{-1}) and Q99L (429 cm^{-1}) show a qualitatively consistent trend relative to experiment. These results indicate that, upon

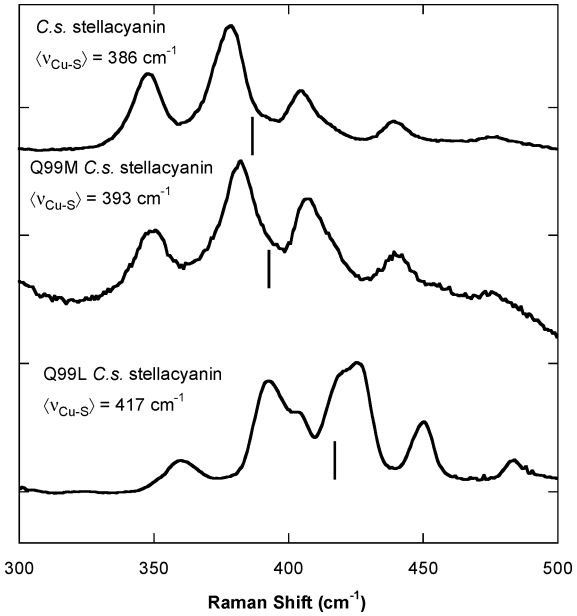

Figure 6. Resonance Raman spectra obtained upon excitation at 647.1 nm for WT, Q99M, and Q99L stellacyanins. Lines mark the position of the intensity-weighted average of the Cu−S vibrations.

reducing the donor strength of the axial ligand, the Cu−S(Cys) bond becomes stronger. This is consistent with both the decrease in the bond length indicated by EXAFS and the increase in covalency indicated by S K-edge XAS.

(E) Absorption and MCD. A comparison of the absorption and MCD spectra for WT, Q99M, and Q99L stellacyanins is shown in Figure 7. Ligand-field and charge-transfer transitions can be differentiated by their relative intensities in absorption and MCD. For MCD, the intensity depends on the magnitude of the spin−orbit coupling for the center involved in the transition.[66,67] Because the spin−orbit coupling parameter for Cu is greater than that for S or N, transitions centered on the Cu (i.e., d → d) will have a higher MCD (*C*-term) intensity than those transitions which involve significant ligand character (i.e., charge transfer (CT)). Alternatively, absorption intensity is much higher for CT transitions because the intensity derives from the ligand−ligand overlap between the donor and acceptor orbitals.

For comparison, the absorption spectra have been normalized to unit intensity at ~16 500 cm^{-1} (600 nm). The absorption spectra are all dominated by an intense S$\pi \rightarrow d_{x^2-y^2}$ CT band at ~16 500 cm^{-1} (Table 3).[68] In addition, there is a weak S pseudo-$\sigma \rightarrow d_{x^2-y^2}$ CT transition at ~19 000 cm^{-1} (arrow).[68] The high-intensity Sπ CT transition and relatively weak S pseudo-σ CT transition indicate that all of these sites are similarly tetrahedral. If the site were to distort tetragonally, the rotation of the HOMO would increase the pseudo-σ interaction and decrease the π interaction of the S(Cys) with the Cu $d_{x^2-y^2}$, resulting in a change in the relative ratios of the intensities of these transitions.[13] The four lower energy transitions, intense in the MCD and weak in the absorption, are assigned to ligand-field transitions. On the basis of analogy to other blue copper sites, these bands are assigned (in order of decreasing energy)

(63) Blair, D. F.; Campbell, G. W.; Schoonover, J. R.; Chan, S. I.; Gray, H. B.; Malmström, B. G.; Pecht, I.; Swanson, B. I.; Woodruff, W. H.; Cho, W. K.; English, A. M.; Fry, H. A.; Lum, V.; Norton, K. A. *J. Am. Chem. Soc.* **1985**, *107*, 5755−5766.
(64) Han, J.; Adman, E. T.; Beppu, T.; Codd, R.; Freeman, H. C.; Huq, L.; Loehr, T. M.; Sanders-Loehr, J. *Biochemistry* **1991**, *30*, 10904−10913.
(65) (a) Badger, R. M. *J. Chem. Phys.* **1934**, *2*, 128. (b) Herschbach, D. R.; Laurie, V. W. *J. Chem. Phys.* **1961**, *35*, 458−463.
(66) Piepho, S. B.; Schatz, P. N. In *Group Theory in Spectroscopy − With Applications to Magnetic Circular Dichroism*; Piepho, S. B., Schatz, P. N., Eds.; John Wiley and Sons: New York, 1983.
(67) Gerstman, B. S.; Brill, A. S. *J. Chem. Phys.* **1985**, *82*, 1212−1230.
(68) Gewirth, A. A.; Solomon, E. I. *J. Am. Chem. Soc.* **1988**, *110*, 3811−3819.

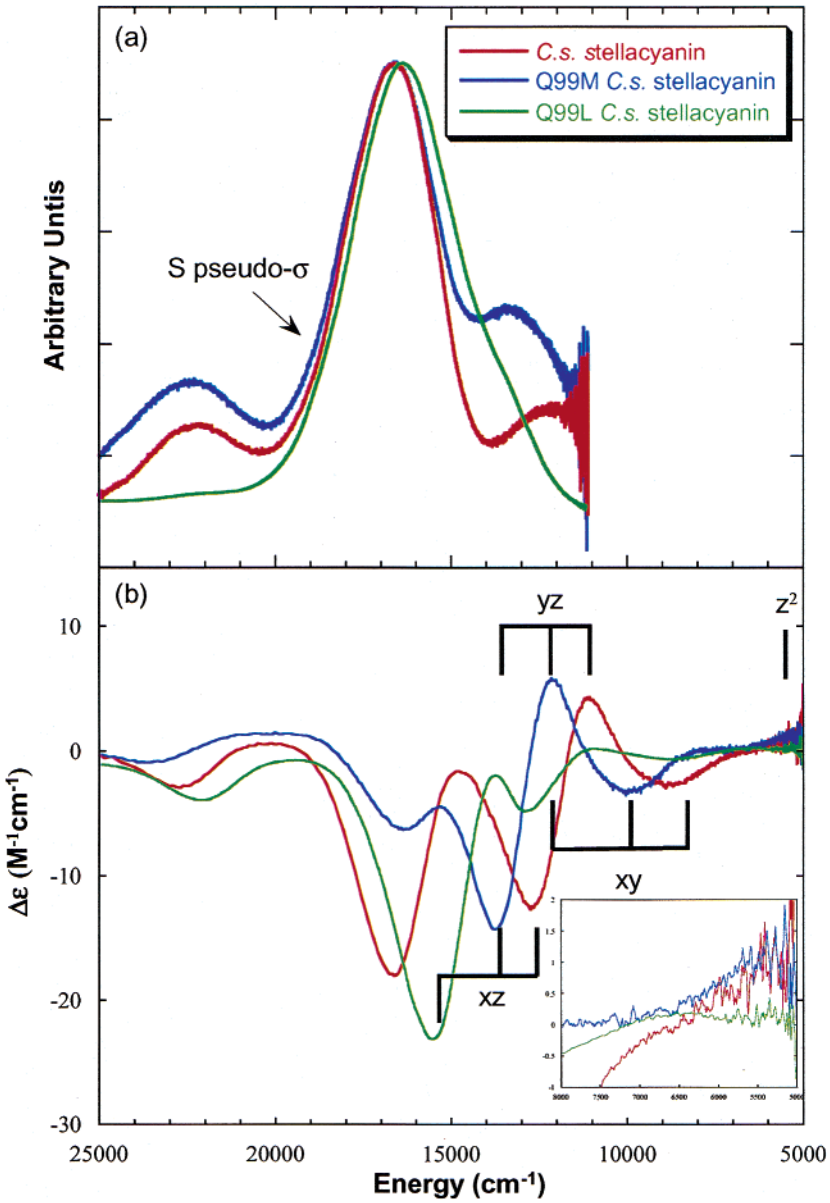

Figure 7. (a) Room-temperature electronic absorption and (b) low-temperature (5 K) MCD of WT, Q99M, and Q99L stellacyanin. Inset shows expanded z^2 region.

Table 3. Absorption and MCD Energies for WT, Q99M, and Q99L Stellacyanin

	energy (cm^{-1})		
band	*C.s.* stellacyanin	Q99M	Q99L
d_{z^2}	5500	5200	6450
d_{xy}	8800	10 000	13 000
d_{xz+yz}	11 200	12 150	14 200
d_{xz-yz}	12 800	13 800	15 600
Cys π	16 800	16 400	16 500
Cys pseudo σ	18 600	19 500	18 300

as $d_{xz} \rightarrow d_{x^2-y^2} > d_{yz} \rightarrow d_{x^2-y^2} > d_{xy} \rightarrow d_{x^2-y^2} > d_{z^2} \rightarrow d_{x^2-y^2}$, as indicated for Q99M stellacyanin.[64] On going from WT to Q99M to Q99L stellacyanin, the energy of these transitions increases, as evidenced by the MCD data and by the low-energy shoulder in the absorption spectra. Quantitatively, the d_{xz} transition increases ~1100 cm^{-1} on going from WT stellacyanin to the Q99M mutant and by ~2000 cm^{-1} on going from the Q99M to Q99L mutant. Hence, as the axial ligand interaction with the Cu(II) is weakened across this series, the equatorial ligand field increases. Because no tetragonal distortion is occurring from the pure Cys π CT spectrum, this indicates that, as the axial ligand is weakened (or removed), the copper shifts into the $(Cys)(His)_2$ plane and the site becomes more trigonally distorted from tetrahedral.

(F) EPR. Figure 8 shows the EPR spectra for WT *C.s.* stellacyanin and the Q99M and Q99L mutants. Table 4 presents the spin Hamiltonian parameters obtained from EPR spectral simulations. The observed g values ($g_{\|} > g_{\perp} > 2.0023$) are consistent with a $d_{x^2-y^2}$ half-occupied highest molecular orbital (HOMO). The g_z value decreases and the A_z value increases on going from WT to Q99M to Q99L stellacyanin. The g value expressions obtained from ligand-field theory are directly proportional to the amount of metal character in the half-occupied HOMO (i.e., covalency) and inversely proportional to the ligand-field transition energies. In the simplest approximation where the ligand does not contribute orbital angular

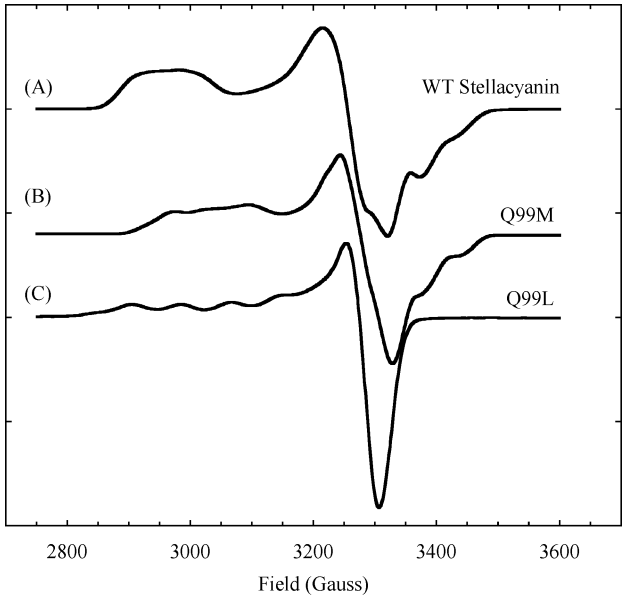

Figure 8. EPR spectra of WT *C.s.* stellacyanin (A), Q99M *C.s.* stellacyanin (B), and Q99L *C.s.* stellacyanin (C). Experimental conditions are the following: microwave power, 10 mW; modulation amplitude 12 G; modulation frequency 100 kHz; time constant 327.68 ms.

Table 4. Spin Hamiltonian Parameters Obtained from EPR Simulations[a]

	g_x	g_y	g_z	A_z
WT	2.03	2.08	2.29	35
Q99M	2.02	2.07	2.24	46
Q99L	2.04	2.05	2.22	80

[a] The $A_{x,y}$ are too small to be reliably estimated.

momentum, the expressions are

$$g_{\|} = 2.0023 - (8\lambda\alpha^2\beta^2)/(E_{xy} - E_{x^2-y^2})$$

$$g_{\perp} = 2.0023 - (2\lambda\gamma^2\beta^2)/(E_{xz,yz} - E_{x^2-y^2}) \qquad (2)$$

where $\lambda(Cu^{II}) = -830$ cm^{-1}, and β, α, and γ are the metal $d_{x^2-y^2}$, d_{xy}, and $d_{xz/yz}$ orbital coefficients in the ligand-field wave functions.[69] $E_{x^2-y^2}$, E_{xy}, and $E_{xz,yz}$ are the ligand-field excited-state energies. Analysis of the d $\rightarrow$ d transitions in the absorption and the MCD spectra shows that on going from WT to Q99M to Q99L stellacyanin, the energy of the ligand-field transitions increases (Figure 7b). Assuming similar metal character in the half-occupied HOMO for WT and the Q99M and Q99L mutants, and using the experimental energy of the $d_{xy} \rightarrow d_{x^2-y^2}$ transition (E_{xy}) (Table 3) and $g_{\|}$ of WT *C.s.* stellacyanin (see Table 4), we predicted the $g_{\|}$ to be 2.25 for Q99M and 2.19 for Q99L. The calculated value for Q99M is close to the experimental value, indicating that the increased ligand-field transition energy accounts for the smaller *g* value. However, for the Q99L mutant, the calculated value is lower than experiment. This indicates that there is an increased contribution from the metal to the half-occupied HOMO in the Q99L mutant relative to the WT (consistent with the analysis of the S K-pre-edge energies).

The $A_{\|}$ value is higher in the two mutants (Q99M $A_{\|} = 46 \times 10^{-4}$ cm^{-1}, Q99L $A_{\|} = 80 \times 10^{-4}$ cm^{-1}) relative to the WT *C.s.* stellacyanin ($A_{\|} = 35 \times 10^{-4}$ cm^{-1}). The hyperfine coupling constants depend on (a) Fermi contact, which is due to the unpaired spin density at the Cu nucleus, (b) direct spin dipolar coupling, which arises from the interaction of the electron spin with the nuclear spin of the metal, and (c) indirect (orbital) dipolar coupling, which is due to coupling of the electron orbital magnetic moment and the nuclear spin of the metal and is related to the deviation of the *g* values (Δg) from 2.0023.

$$A_{\|} = P_d((-\kappa - {}^4/_7)\alpha^2 + {}^3/_7\Delta g_{\perp} + \Delta g_{\|})$$

$$A_{\perp} = P_d((-\kappa + {}^2/_7)\alpha^2 + {}^{11}/_{14}\Delta g_{\perp}) \qquad (3)$$

P_d is 396 $\times$ 10^{-4} cm^{-1}, κ is the Fermi contact term, and α^2 is the percent metal character in the $d_{x^2-y^2}$ orbital.[69]

The change in experimental *g* values can be used to calculate the associated change in hyperfine coupling due to the orbital dipolar term. The decrease in *g* values on going from WT to Q99M accounts for an increase in $A_{\|}$ to 54 $\times$ 10^{-4} cm^{-1}, in agreement with experiment. (Because the orbital dipolar term is positive while the spin dipolar and Fermi contact contributions are negative, $A_{\|}$ is negative.) For the Q99L mutant, when the experimental *g* values are used, the magnitude of $A_{\|}$ increases to -64×10^{-4} cm^{-1}. Thus, the decrease in *g* values accounts for about 60% of the difference in hyperfine coupling between WT and Q99L. The remaining increase in $|A_{\|}|$ is accounted for by the small increase in metal contribution (α^2) to the HOMO verified by the $g_{\|}$ value.

In summary, on going from WT to Q99M to Q99L stellacyanin, the Cu moves into the Cys(His)$_2$ plane, and the ligand-field transitions increase in energy. This results in a decrease in *g* values and an increase in *A* values. Analysis of the *g* values indicates that the metal character does not decrease and actually increases slightly for Q99L stellacyanin. It is interesting to note that even though the S(Cys) character increases across this series, the $A_{\|}$ increases, while the metal character remains constant or increases. Thus, the increase in thiolate character is mostly compensated for by a decrease in histidine character. This is consistent with the changes observed in calculations on stellacyanin, plastocyanin,[13] and fungal laccase,[22] and also parallels trends observed in blue copper model studies where a significant change in the thiolate contribution to the HOMO was observed with no change in metal character.[70]

(G) Density Functional Calculations. The crystallographically based computational model of the stellacyanin active site and its ground-state bonding description by means of natural population analysis (NPA(4p)) are presented in Figure 9. The calculated ground-state wave function obtained using the adjusted Xα-sw method has already been reported[14] to be 57% Cu, 30% S, and 7% N, which corresponds to a too ionic bonding description relative to the S covalency of 41% determined by XAS (vide supra). The spectroscopically adjusted DFT calculations employing the B(38HF)P86 functional, with a theoretically converged basis set (BS5), give a ground-state bonding description in reasonable agreement with experimental covalencies (within 2%). The bonding between the Cu and the S(Cys) π is similar to the Xα-sw results with a small σ/π ratio (0.06, referring to the ratio of S 3p character of the atomic spin density along/perpendicular to the Cu$-$S(Cys) vector), in agreement

(69) McGarvey, B. R. In *Transition Metal Chemistry*; Carlin, B. L., Ed.; M. Dekker: New York, 1966; pp 89$-$201.

(70) Randall, D. W.; George, S. D.; Holland, P. L.; Hedman, B.; Hodgson, K. O.; Tolman, W. B.; Solomon, E. I. *J. Am. Chem. Soc.* **2000**, *122*, 11632$-$11648.

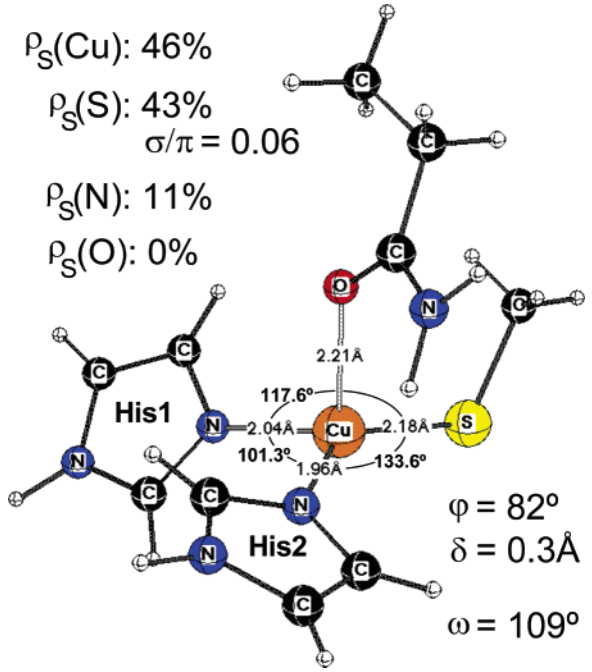

Figure 9. Initial model structure for optimization based on the experimental structure of the stellacyanin active site.

with absorption spectroscopy. There is no contribution found in either calculation from the axial Gln ligand. These computational results validate the use of the B38HFP86 functional in geometry optimization, where the protein environment is taken into account through various constraints on a small model of the active site.

The geometrical parameters of stellacyanin (Figure 9), such as the angle of the N(His)−Cu−N(His) and O(Gln)−Cu−S(Cys) planes ($\varphi = 82°$) and the Cu out-of-plane distance ($\delta = 0.3$ Å), are consistent with a trigonally distorted, tetrahedral structure, which is characteristic of blue, Type 1 Cu sites. Interestingly, the S−Cu−N bond angles (118° and 134°) show some deviation (~16°) from each other, which can be rationalized by the insertion of the N group of the amide ligand between the S(Cys) and N(His2) atoms, which is indicated by the relatively short distance (2.5 Å) of the proximal amide H to N(His2).

With respect to the protein environment of the axial amide ligand, the two closest hydrogen-bonding contacts are found at 3.6 and 3.7 Å, which are between the distal H atom of the amide NH_2 group and a Trp backbone carbonyl O atom, and between the coordinated O of the amide ligand and a H atom on a γC-(Val), respectively. These contacts cannot be considered as strong interactions; therefore, the Gln residue is not constrained by any means other than the backbone αC atom.

When the geometry of a $[(C_3N_2H_4)_2Cu^{II}(SCH_3)(OC(NH_2)C_2H_5)]^+$ model of the stellacyanin active site is fully optimized, it distorts to a tetragonal structure. Figure 10 shows the unconstrained optimization pathway (green line terminated with a diamond) of the model complex starting from the experimental coordinates of the WT stellacyanin active site (Figure 10, 0.0 kcal mol^{-1}, offscale at top). After the initial structural relaxation (steps 1−10), the optimization proceeds through a plateau (steps 13−35), which corresponds to trigonally distorted tetrahedral structures ($\varphi > 80°$, and $\sigma/\pi < 0.2$) with unchanged Cu−S and Cu−O bond lengths (Figures S1 and S2) relative to the experimental geometry, but more equal Cu−N bond lengths of 2.00 Å (Figure S3). Around step 35, the thiolate methyl group starts to rotate around the Cu−S bond with the axial glutamine approaching the Cu center, and the model complex gradually transforms into a tetragonal structure ($\varphi < 50°$, and $\sigma/\pi \gg 1.0$, diamond in Figure 10), which is a true equilibrium geometry (with no imaginary frequency). In this tetragonal structure (Figure 11A), the Cu−S bond is about 0.1 Å longer and the Cu−O bond is about 0.2 Å shorter, relative to the crystal structure, which is associated with the tetrahedral-to-tetragonal coupled distortion. In addition, the N(His)−Cu−N(His) angle decreases to 94° (Figure S4), and the two S(Cys)−Cu−N(His) angles became very different (95° and 149°, Figure S5) as a consequence of the two imidazole ligands being in cis and trans positions relative to the thiolate ligand.

The above rotation of the thiolate methyl group around the Cu−S bond would impose a significant distortion force on the protein backbone through the cysteine residue. Therefore, this rotation was constrained by fixing the C(Cys)−S(Cys)−Cu−N(His) dihedral angles to ±108° as in the crystal structure. The optimization of the constrained active site model takes a different path (Figure 10, red line terminated with a triangle). It also goes through a plateau (steps 17−30), which is different from the path of the unconstrained optimization pathway (Figure 10, green line, steps 13−35). This plateau is related to a slow change of the nonequal Cu−N(His) distances (Figure S3) and rotation of the imidazole ligands around the Cu−N(His) bonds; however, the structure of the model complex remains similarly trigonally distorted tetrahedral along the whole path. The steep drop between steps 33 and 38 corresponds to the process of the Cu−N(His) bonds becoming equal (Figure S3) along with correlated changes in the S−Cu−N(His) angles (Figure S5). The constrained optimization converges to a stationary point (Figure 11B, triangle in Figure 10) with one small imaginary frequency (−10 cm^{-1}), which is a correlated rotation around the Cu−S bond and concomitant movement of the axial amide group. In this stationary point, the Cu−N(His) distances are equal (2.02 Å), and the Cu−S(Cys) and Cu−O(Gln) bond lengths are identical to the experimental values within the accuracy (1.6-Å resolution) of the protein crystal structure.[17] The structure in Figure 11B is similar to the active site structure of stellacyanin.

By using the structure in Figure 11B, where internal coordinates not involving the Cu center are at their optimal values, we could calculate the relative energy of the experimental active site structure. By adjusting the bond lengths, bond angles, and torsions around the Cu atom to match those of the experimental structure, the total energy increases by 4.5 kcal mol^{-1} in going from the partially optimized structure in Figure 11B to the experimental/initial structure in Figure 9, which can be broken into individual contributions of 0.6, 2.0, and 1.9 kcal mol^{-1}, respectively.

The trigonally distorted tetrahedral stationary point (Figure 11B) can be directly transformed to the tetragonally distorted equilibrium geometry (Figure 11A) by allowing the two constrained dihedral angles of C(Cys)−S(Cys)−Cu−N(His) to relax (Figure 10, brown line, pathway connecting triangle with diamond).

Note that the above constraints are not unique and there are other pathways related to those in Figure 10 that also converge to lower energy tetragonal sites. Other constraints can be

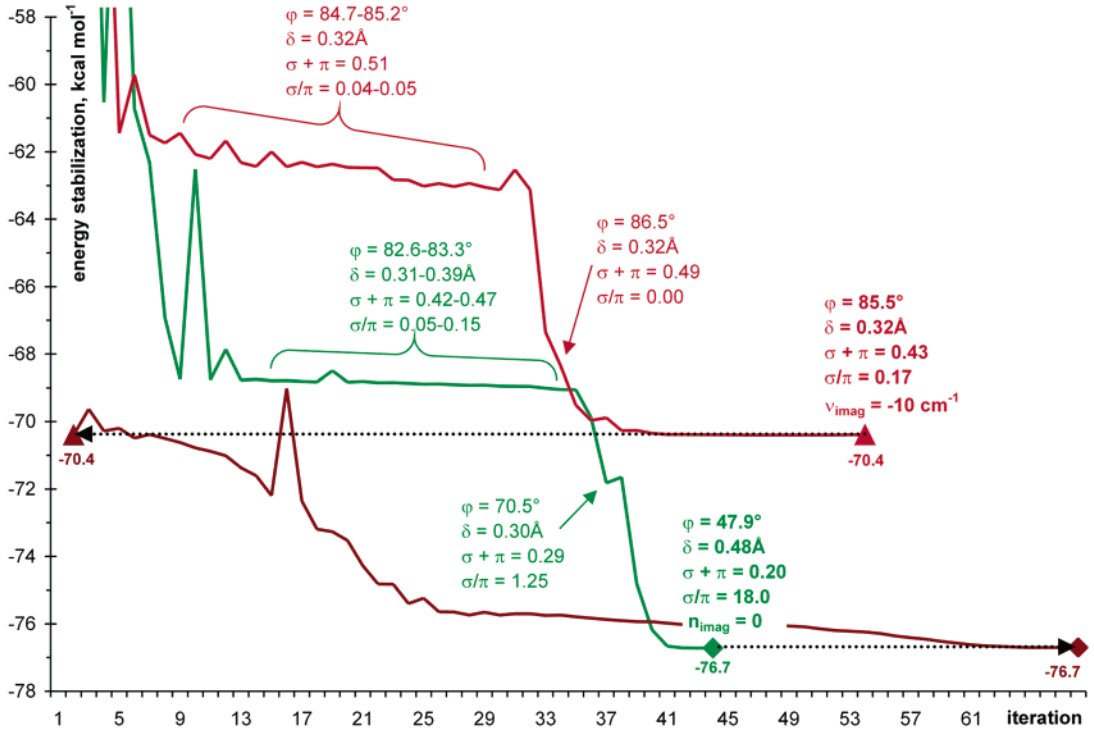

Figure 10. Geometric optimization pathways of the stellacyanin model structure calculated at B(38HF)P86/BS5 level of theory (green line, unconstrained optimization; red line, constrained optimization with fixed C(Cys)−S(Cys)−Cu−N(His1/His2) torsions; brown line, optimization path connecting the constrained stationary point with the equilibrium structure).

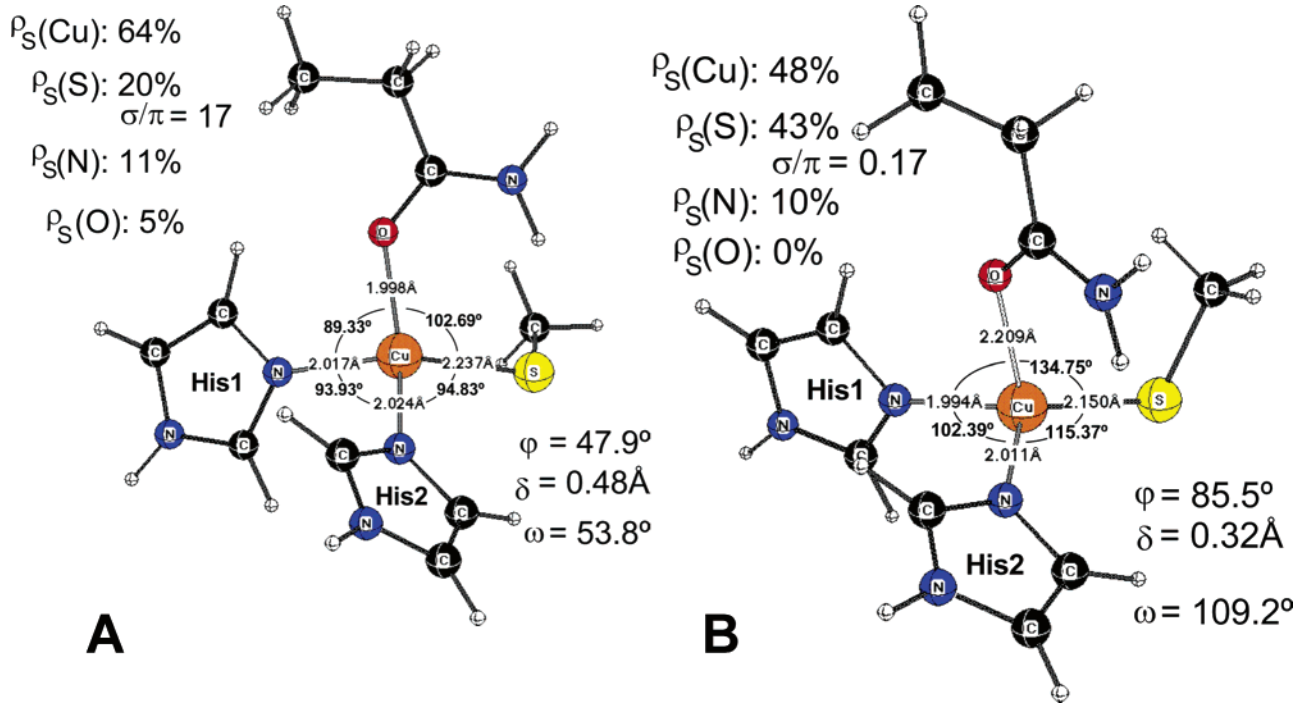

Figure 11. Equilibrium geometry (A, diamond in Figure 9) and stationary point (B, triangle in Figure 9) of the constrained optimization of stellacyanin model structure $[(C_3N_2H_4)_2Cu^{II}(SCH_3)\ (OC(NH_2)C_2H_5)]^+$ at B(38HF)P86/BS5 level of theory.

imposed as well, in particular, fixing the Cu−O(Gln) bond or the S(Cys)−Cu−N(His2) angle, which in addition to the C(Cys)−S(Cys)−Cu−N(His) dihedral angles show the largest changes along the unconstrained optimization pathway. In both cases, the constrained optimizations lead directly to a tetragonally distorted geometry with a high σ/π ratio. The optimization with fixed Cu−O(Gln) distance at 2.21 Å gives a stationary point (with $\sigma/\pi = 17$) highly similar to the equilibrium structure of the unconstrained optimization (Figure 11A); however, it is ∼2 kcal mol^{-1} higher in energy due to the Cu−O(Gln) constraint. Interestingly, the optimization with a constrained S(Cys)−Cu−N(His2) angle at 134° leads to a stationary point with a tetragonally flattened tetrahedral structure (with 17−25° out-of-plane angles of the ligands as compared to 35° in an ideal tetrahedron) with the S(Cys)−C(Cys) vector perpendicular to the approximate equatorial plane of the complex. Once the

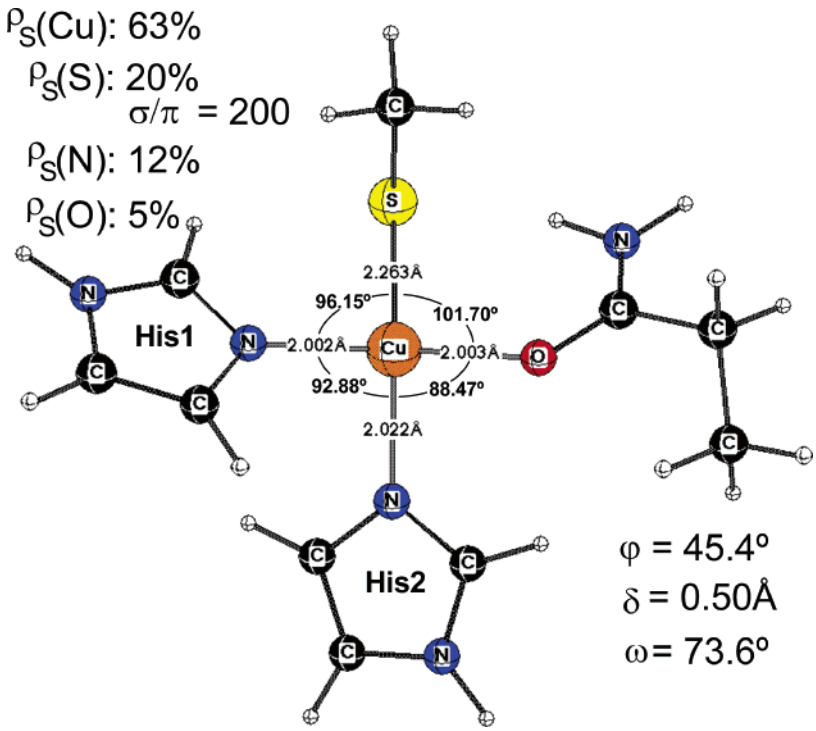

Figure 12. Equilibrium geometry of the tetragonal model structure of the stellacyanin active site.

constraint is released, the S(Cys)−Cu−N(His) angle opens up to 149°, and the geometry becomes similar to the fully optimized structure in Figure 11A; however, the perpendicular thiolate and glutamine ligands have switched their positions (Figure 12). This structural difference corresponds to an energetically slightly lower equilibrium structure by 2 kcal mol^{-1} relative to that in Figure 11A.

These computational results indicate that, without any restraints, the tetrahedral active site of the WT stellacyanin distorts to a tetragonal structure, which, however, requires large angular changes in the thiolate or the glutamine positions. The two histidine ligands stay fairly unperturbed relative to their crystal structure positions, but they rotate around the Cu−N bonds. On the basis of geometry optimizations with fixed S(Cys)−Cu−N(His) and C(Cys)−S(Cys)−Cu−N(His) internal coordinates, it seems that the surrounding protein matrix constrains the trigonally distorted tetrahedral structure through the position of the axial glutamine ligand, and the rotation of the Cu−S(Cys) bond is simply a response to an unconstrained bulky axial ligand approaching the Cu center. This constraint is worth ∼7 kcal mol^{-1} as estimated from the structural relaxation due to the rotation of the thiolate methyl group around the Cu−S bond (Figure 10, brown line).

IV. Discussion

The results of this study show that the axial donor interaction with the Cu decreases upon changing the axial ligand from O(Gln) to S(Met) to no axial ligand (leucine). This is demonstrated by Cu K-edge XAS results on the oxidized proteins, which show an ∼0.5 eV increase in the 1s → 3d pre-edge transition energy on going from WT stellacyanin to the Q99M mutant, indicating a weaker donor. In addition, Cu K-edges of the reduced proteins show an increase in the intensity of the 1s → 4p 8984 eV transition on going from WT stellacyanin to the Q99M and Q99L mutants, again consistent with a weaker donor interaction. EPR data indicate that the Cu 3d character in the HOMO does not decrease across the series and may actually increase slightly. This is supported by S K-edge XAS energy analysis, which indicates an increase in Z_{eff} across this series. On the basis of XAS, optical, resonance Raman, and EPR data, the Q99M mutant appears to accurately reproduce the geometric and electronic properties of the classic blue copper sites in azurin and plastocyanin. For Q99L, optical, resonance Raman, and EPR data suggest the site well models the T1 site of fungal laccases. This series thus covers the range of known axial ligands in WT blue copper sites and allows for assessment of the axial ligand contributions to the geometric and electronic properties of the active site in a fixed protein environment.

The results of this study clearly demonstrate that the axial ligand modulates both the geometric and the electronic structure of the oxidized blue copper site. EXAFS data on the oxidized proteins show that on going from WT to Q99M to Q99L stellacyanin, the Cu−S bond length decreases by 0.04−0.05 Å. This indicates that, as the axial bond is weakened, the Cu−S(thiolate) becomes shorter. These results are supported by resonance Raman results which show an increase in the Cu−S(thiolate) stretching frequency upon weakening the axial ligand. S K-edge XAS results also clearly show that, as the axial ligand is weakened, the covalency of the Cu−S(thiolate) bond increases. Upon changing the axial ligand from O(Gln) to S(Met) to no axial (Leu), the covalency increases from 41% to 47% to 54% S 3p character. This trend is further supported by the increase in intensity of the oxidized Cu K-edge 1s → 4p + shakedown transition on going from WT to Q99M stellacyanin. However, XAS pre-edge energies (and EPR) show that the effective nuclear charge on the copper increases on going from O(Gln) to S(Met) to no axial (Leu), indicating that the weakening of the axial ligand is not fully compensated for by the increased donation from the thiolate. Finally, MCD studies

show that, upon weakening the axial ligand, the equatorial ligand field increases. Because there is no tetragonal distortion of the site (i.e., no increase in Cys σ CT intensity), this indicates that the Cu shifts into the S(Cys)N(His)$_2$ plane as the axial ligand strength decreases, thus becoming a more trigonally distorted tetrahedral site.

The changes in geometric and electronic structure, which result from variation in the axial ligand, can make important contributions to ET properties of blue copper sites. There are three factors to consider: the donor−acceptor electronic coupling (H_{DA}), the reorganization energy (λ), and the redox potential ($E°$). All three factors contribute to the kinetics of ET.[71−75] Changes in $E°$ are also important for tuning the protein site to function efficiently in its electron transport chain.

Going from WT to Q99M to Q99L stellacyanin, the covalency of the Cu−S(Cys) bond increases from 41% to 47% to 54% S 3p character. This change will result in a small increase in H_{DA} across the series, providing somewhat better coupling into ET pathways (which goes as $(H_{DA})^2$ for nonadiabatic ET).[12,76−78] Modulation of the axial ligand may also contribute to the inner-sphere reorganization energy (λ_i). Across the series (going from WT to Q99M to Q99L stellacyanin), the length of the Cu−S(Cys) bond decreases in the oxidized proteins; however, in the reduced protein it remains the same. In addition, the resonance Raman data show that the force constant increases across this series. The increased geometric change and higher force constant should result in an increased contribution of the Cu−S(Cys) bond to the inner-sphere reorganization energy of these sites. Using the intensity weighted Cu−S frequency, $\langle\nu_{Cu-S}\rangle$, from the resonance Raman spectra we could obtain a force constant for the oxidized site ($k_{Cu-S(oxidized)}$) and use it to estimate a force constant for the reduced site ($k_{Cu-S(reduced)}$). The contribution of the Cu−S(Cys) bond length change to the reorganization energy can then be estimated from eq 4:

$$\lambda_{Cu-S} = [k_{Cu-S(oxidized)} * k_{Cu-S(reduced)}]/[k_{Cu-S(oxidized)} + k_{Cu-S(reduced)}](\Delta R_{Cu-S})^2 \quad (4)$$

where ΔR_{Cu-S} is the change in the Cu−S bond length upon reduction of the site.[72,79] This results in an increase by a factor of ∼1.5 in λ_{Cu-S} on going from WT to Q99M stellacyanin, and an increase of by a factor of ∼2 on going from Q99M to the Q99L mutant. Previous studies on plastocyanin estimate that the change in the Cu−S(Cys) bond contributes 85−90% of the inner-sphere reorganization energy.[80] Thus, the histidines make a small and similar contribution in all three proteins on the basis of the EXAFS results. Hence, if only the three equatorial ligands are considered, the inner-sphere reorganization energy increases across this series. However, the contribution from the axial ligand must also be considered. For the methionine and the leucine, the contribution to λ_i is likely insignificant. However, for WT stellacyanin, crystallographic results show an ∼0.5 Å increase in the Cu−O(Gln) bond length upon reduction.[81] Using a force constant of 1.3 mdyn/Å as an estimate for a Cu(II)−O bond at 2.2 Å[82] and Badger's rule[65] to estimate a force constant for the reduced site (∼0.3 mdyn/Å) results in a λ_{Cu-O} of ∼0.2 eV. This is a factor of 2 increase in the inner-sphere reorganization energy relative to plastocyanin. Hence, the smaller change in the Cu−S distance in WT stellacyanin is offset by the change in the axial ligand, and all three sites maintain reasonably low inner-sphere reorganization energies.[83]

Experimentally, the redox potential increases from 260[26] to 420[26] to 580 mV (Figure S6) on going from WT to Q99M to Q99L stellacyanin, clearly indicating that the axial ligand modulates the redox potential of the site within a fixed protein environment.[10,84] However, it should also be noted that, among the wild-type fungal laccases, the redox potential for the T1 site ranges from 465 to 778 mV,[18,85]and for classic blue copper sites with axial S(Met), the redox potential ranges from 250 to 680 mV.[86,87] This indicates that, while the axial ligand makes a significant contribution to the redox potential, the protein matrix also tunes the potential over a wide range. There are four primary active site contributions to the redox potential: geometric relaxation, electronic relaxation, the energy of the redox active molecular orbital (RAMO), and the change in the effective nuclear charge (Z_{eff}).[88] The changes in geometric and electronic structure of blue copper sites upon reduction are small.[10] The energy of the RAMO is determined primarily by the ligand field, which from the MCD data in Figure 7 increases across this series (going from WT to Q99M to Q99L stellacyanin). The increase in the ligand field raises the energy of the RAMO, which would lower $E°$. However, experimentally, $E°$ increases across this series. This is due to the increase in Z_{eff}, which lowers the d-manifold energy and increases $E°$. The increased Z_{eff} results from the weakened axial ligand which is not fully compensated by the increased donation from the Cu−S(thiolate) bond. This is qualitatively observed through analysis of the XAS edge energies and is also consistent with EPR results. Across the series (WT to Q99M to Q99L stellacyanin), the S K-edge energy stays the same. However, from MCD spectroscopy, the ligand field increases by 0.13 and 0.38 eV relative to WT, for Q99M and Q99L stellacyanin, respectively. This requires that the effect of the change in Z_{eff} on the d orbital

(71) Marcus, R. A.; Sutin, N. *Biochim. Biophys. Acta* **1985**, *811*, 265−322.
(72) Newton, M. D. *Chem. Rev.* **1991**, *91*, 767−792.
(73) Beratan, D. N.; Betts, J. N.; Onuchic, J. N. *Science* **1991**, *252*, 1285−1288.
(74) Beratan, D. N.; Hopfield, J. J. *J. Am. Chem. Soc.* **1984**, *106*, 6, 1584−1594.
(75) Beratan, D. N.; Onuchic, J. N.; Hopfield, J. J. *J. Chem. Phys.* **1987**, *86*, 4488−4498.
(76) Machonkin, T. E.; Solomon, E. I. *J. Am. Chem. Soc.* **2000**, *122*, 12547−12560.
(77) George, S. D.; Metz, M.; Szilagyi, R. K.; Wang, H. X.; Cramer, S. P.; Lu, Y.; Tolman, W. B.; Hedman, B.; Hodgson, K. O.; Solomon, E. I. *J. Am. Chem. Soc.* **2001**, *123*, 5757−5767.
(78) Regan, J. J.; DiBilio, A. J.; Langen, R.; Skov, L. K.; Winkler, J. R.; Gray, H. B.; Onuchic, J. N. *Chem. Biol.* **1995**, *2*, 489−496.
(79) Because EXAFS data indicate that the Cu−S bond lengths are the same for all three reduced proteins, $k_{Cu-S(reduced)}$ is assumed to be the same for WT, Q99M, and Q99L stellacyanin.
(80) (a) Fraga, E.; Webb, M. A.; Loppnow, G. R. *J. Phys. Chem.* **1996**, *100*, 3278−3287. (b) Webb, M. A.; Kwong, C. M.; Loppnow, G. R. *J. Phys. Chem. B* **1997**, *101*, 5062−5069.
(81) Nersissian, A. M.; Hart, J. P.; Valentine, J. S. In *Handbook of Metalloproteins*; Messerschmidt, A., Huber, R., Poulos, T., Wieghardt, K., Eds.; John Wiley and Sons: Chichester, 2001; pp 1219−1234.
(82) Campos-Vallette, M.; Figueroa, K.; LaTorre, R. O.; Diaz Fleming, G.; Costamagna, J.; Canales, J. C.; Rey-Lafon, M.; Derouault, J. *Vib. Spectrosc.* **1993**, *6*, 25−35.
(83) Experimentally, the total reorganization energy for stellacyanin is 1.4 times greater than that of plastocyanin. However, this has been attributed to the more exposed nature of the site, which increases the outer sphere contribution to λ (Farver, O.; Pecht, I. *Inorg. Chem.* **1990**, *29*, 4855−4858).
(84) Malmström, B. G.; Leckner, J. *Curr. Opin. Chem. Biol.* **1998**, *2*, 286−292.
(85) Malmström, B. G.; Reinhammer, B.; Vänngård, T. I. *Eur. J. Biochem.* **1971**, *18*, 463−468.
(86) Diederix, R. E.; Canters, G. W.; Dennison, C. *Biochemistry* **2000**, *39*, 9551−9560.
(87) Ingeledew, W. J.; Cobley, J. G. *Biochim. Biophys. Acta* **1980**, *590*, 141−158.
(88) Kennepohl, P.; Solomon, E. I. *Inorg. Chem.* **2003**, *42*, 689−695.

energy is at least as great as the change in ligand field. The change is Z_{eff} is likely even larger due to a shift in the sulfur 1s core to deeper binding energy upon increasing the covalency of the Cu−S(thiolate) bond. By analogy to the core shift on going from a thiolate to sulfide (~0.8 eV),[89] it is estimated that the core could shift by up to 0.2 eV between WT and Q99L stellacyanin. These results clearly show the change in Z_{eff} is the dominant contribution to the change in $E°$.

The results of this study demonstrate that variation of the axial ligand allows the blue copper site to maintain good electronic coupling into the protein superexchange pathways and a low inner-sphere reorganization energy providing for facile ET, while still tuning the redox potential to a biologically relevant range.

The Q99M and Q99L mutants are spectroscopically similar to plastocyanin and the T1 site of fungal laccase, respectively. As the axial ligand is weakened, the sites remain trigonally distorted tetrahedral. However, WT stellacyanin, with a strong axial O(Gln), does not undergo a tetragonal distortion. This is in contrast to the blue copper sites in nitrite reductase and cucumber basic protein which have stronger axial Met bonds than plastocyanin (i.e., shorter Cu−S(Met) bond lengths) and show a tetragonal distortion.[13,14] Previous studies have suggested that in stellacyanin the protein structure could limit the Jahn−Teller tetragonal distortion and the site remains distorted tetrahedral.[14] The computational results in this study do in fact indicate that, when fully optimized, the active site of stellacyanin undergoes a tetragonal distortion. This distortion requires a large change in the thiolate and glutamine positions, indicating that the protein may make a significant contribution to maintaining the trigonally distorted tetrahedral structure of the stellacyanin active site.

In summary, the results of this study show that Q99M and Q99L stellacyanin are good models for plastocyanin and the T1 site in fungal laccase, respectively. Modulation of the axial ligand allows the protein to tune the redox potential of the site, while maintaining good donor−acceptor electron coupling and a low inner-sphere reorganization energy to provide for rapid ET. DFT calculations on WT stellacyanin show that the protein environment is an important factor in stabilizing the structure relative to a Jahn−Teller distorted tetragonal site.[90]

Acknowledgment. We thank Dr. Steven Berry and Prof. Yi Lu for providing the *P.a.* azurin samples, and the Clark Center at Stanford and the Bio-X program for computational time on a Silicon Graphics Orgin 3800 shared memory supercomputer. This work was supported by NSF CHE-9980549 (E.I.S.), NIH RR-01209 (K.O.H), and NIH GM28222 (J.S.V.). SSRL operations are funded by the Department of Energy, Office of Basic Energy Sciences. The Structural Molecular Biology program is supported by the National Institutes of Health, National Center for Research Resources, Biomedical Technology Program and by the Department of Energy, Office of Biological and Environmental Research.

Supporting Information Available: Plots showing changes in the stellacyanin model parameters along the optimization pathways of the calculations. Cylic voltammetry of Q99L stellacyanin (PDF). This material is available free of charge via the Internet at http://pubs.acs.org.

JA035802J

(89) Rose, K.; Shadle, S. E.; Glaser, T.; de Vries, S.; Cherepanov, A.; Canters, G. W.; Hedman, B.; Hodgson, K. O.; Solomon, E. I. *J. Am. Chem. Soc.* **1999**, *121*, 2353−2363.

(90) The equilibrium (Figure 11A) and the point stationary (Figure 11B) geometries calculated by B(38HF)P86 functional are different from the structures calculated at the B3LYP level by De Kerpel et al. (De Kerpel, J. O. A.; Pierlot, K.; Ryde, U.; Roos, B. O. *J. Phys. Chem. B* **1998**, *102*, 4638−4647). In their calculations, both tetragonal and trigonal structures are minima on the potential energy surface and are degenerate within 0.5 kcal mol^{-1} in energy. The trigonally distorted tetrahedral structure is similar to the structures on the plateau of the constrained optimization (Figure 10, red line, steps 17−30) with nonequal Cu−N distances. Their tetragonal structure does not compare directly with any point of the optimization pathways discussed here, because the arrangement of the ligands are different.